

Contrails

**WIND TUNNEL TESTS
OF
A FREE-WING TILT-PROPELLER V/STOL AIRPLANE MODEL**

**T. STRAND
E. S. LEVINSKY, Ph. D.**

**This document has been approved for public release and sale:
its distribution is unlimited.**

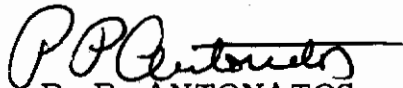
FOREWORD

The research reported upon in this document was conducted under Air Force Contract F33615-68-G-1672, "Wind Tunnel Tests of a Free-Wing Tilt-Propeller V/STOL Airplane Model," by Air Vehicle Corporation, San Diego, California. Sponsorship was by the Air Force Flight Dynamics Laboratory (AFFDL), Air Force Systems Command, Wright-Patterson Air Force Base, Ohio and by the Naval Ship Research and Development Center, Washington, D. C.

Work was initiated in June 1968 and completed in August 1969. Mr. Russel F. Osborn, FDMM Project Engineer, was the contract technical monitor for the Air Force.

The experiments were concluded in July 1969 and this report was released by the authors October 1969 for publication as an R&D Technical Report.

This technical report has been reviewed and is approved.



P. P. ANTONATOS
Chief, Flight Mechanics Division
Air Force Flight Dynamics Laboratory

ABSTRACT

Wind tunnel tests have been conducted on a free-wing tilt-propeller V/STOL airplane model to investigate the aerodynamic characteristics of the free-floating wing in the propeller slipstream through the transitional region from cruise to near hover. Lift and drag curves wing-free have been obtained as a function of propeller tilt angle and thrust coefficient, and are compared with wing-pinned data.

The results indicate that the tilted propeller does not significantly turn the flow past the wing, except at thrust coefficients near unity and at propeller tilt angles near 90° . It is found that lift curve slope and maximum lift coefficient are strong functions of thrust coefficient. Provided the cruise static margin is adequate, the free-floating wing with flap and slat retracted behaves in the slipstream with no unusual problems. Based upon these initial test results, the free-wing concept therefore appears to be feasible aerodynamically. Additional wind tunnel tests are required on the free wing with flap and slat extended.

This document has been approved for public release and sale; its distribution is unlimited.

TABLE OF CONTENTS

<u>Title</u>	<u>Page</u>
INTRODUCTION	1
TEST FACILITIES	2
MODEL	2
RESULTS AND DISCUSSION	5
REFERENCES	13

LIST OF ILLUSTRATIONS

<u>Figure</u>	<u>Title</u>	<u>Page</u>
1	Three-view of wind tunnel model	15
2a	Semispan model in the LTV wind tunnel	16
2b	Semispan model in the AARL wind tunnel	17
3	Airfoil sections	18
4	Model support block, fuselage balance support block wing oscillation damper assembly (not used), nacelle support shaft, and wing support shaft	19
5	Effect of pivot location and wing trailing edge angle on lift (wing free, flaps and slat retracted, $Re \approx 0.35 \cdot 10^6$, LTV tunnel, $q_\infty = 6$).	20
	Effect of pivot location and wing trailing edge angle on drag	21
6	Lift (flap and slat retracted, propeller off, T.E. 2, $\delta_3 = 0$, $Re \approx 0.35 \cdot 10^6$, pivot at 0.198 c, LTV tunnel, $q_\infty = 6$) . .	22
	Pitching moment and drag.	23
7	Lift (wing free, flap and slat retracted, T.E. 2, $\delta_3 = 0$, $Re \approx 0.35 \cdot 10^6$, pivot at 0.198 c, LTV tunnel).	24
	Drag polars	25
8	Lift (wing free, flap and slat retracted, T.E. 2, $\delta_3 = 0$, $Re \approx 0.35 \cdot 10^6$, pivot at 0.198 c, LTV tunnel).	26
	Drag polars	27
9	Lift (wing free, flap and slat retracted, T.E. 2, $\delta_3 = 0$, $Re \approx 0.35 \cdot 10^6$, pivot at 0.198 c, LTV tunnel).	28
	Drag polars	29

LIST OF ILLUSTRATIONS (Continued)

<u>Figure</u>	<u>Title</u>	<u>Page</u>
10	Lift (wing free, flap and slat retracted, T.E. 2, $\delta_3 = 0$, $Re \approx 0.35 \cdot 10^6$, pivot at 0.198 c, LTV tunnel).	30
	Drag polars	31
11	Lift (wing free, flap and slat retracted, T.E. 2, $\delta_3 = 0$, $Re \approx 0.35 \cdot 10^6$, pivot at 0.198 c, LTV tunnel).	32
	Drag polars	33
12	Lift (wing free, flap and slat retracted, T.E. 2, $\delta_3 = 0$, $Re \approx 0.35 \cdot 10^6$, pivot at 0.198 c, LTV tunnel).	34
	Drag polar	35
13	Lift comparison at two different dynamic pressures in two wind tunnels (wind pinned, flap and slat retracted, propeller off, T.E. 1, $\delta_{123} = 0$).	37
14	Lift (flap and slat retracted, T.E. 3, $\delta_{13} = 0$, $Re_{\text{pinned}} \approx 0.82 \cdot 10^6$, pivot at 0.216 c, AARL tunnel)	38
	Pitching moment and drag	39
15	Lift, pitching moment, and drag (wing pinned, flap and slat retracted, T.E. 3, $\delta_3 = 0^\circ$, $Re \approx 0.25 \cdot 10^6$, pivot at 0.216 c, AARL tunnel, $q_\infty = 2$).	40
16	Lift (wing free, flap and slat retracted, T.E. 3, $\delta_{13} = 0$, $Re \approx 0.3 \cdot 10^6$, pivot at 0.216 c, AARL tunnel)	41
17	Lift (wing free, flap and slat retracted, T.E. 3, $\delta_{13} = 0$, $Re \approx 0.3 \cdot 10^6$, pivot at 0.216 c, AARL tunnel)	42
18	Lift and pitching moment (flap and slat extended, propeller off, T.E. 4, $\delta_3 = -12.5^\circ$, $Re \approx 1.18 \cdot 10^6$, pivot at at $\sim 0.22 c$ extended, AARL tunnel, $q_\infty = 20$)	43

LIST OF ILLUSTRATIONS (Continued)

<u>Figure</u>	<u>Title</u>	<u>Page</u>
19	Lift (wing free, flap and slat extended, T.E. 4, $\delta_3 = -12.5^\circ$, $Re \approx 0.52 \cdot 10^6$, pivot at $\sim 0.22 c_{\text{extended}}$ AARL tunnel, $q_\infty = 4$)	44
20	Propeller thrust offset distance at angles of tilt	45

Contrails

SYMBOLS

Note: All forces are referred to wind axes.

α	wing angle of attack, measured from the free stream direction
α_p	propeller angle of attack, measured from free stream direction
A	propeller area
c	wing chord, flap and slat retracted
\bar{C}_D	wing drag coefficient [= $D/S (q_\infty + T/A)$]
\bar{C}_L	wing lift coefficient [= $L/S (q_\infty + T/A)$]
\bar{C}_M	wing pitching moment coefficient about pivot [= $M/S c (q_\infty + T/A)$]
δ	tab deflection angle, positive trailing edge down (δ_1 inboard tab, δ_2 center tab, δ_3 outboard tab, δ_{12} inboard and center tab connected)
D	drag of wing panel
e	aerodynamic efficiency factor
L	lift of wing panel
M	wing pitching moment about pivot, positive nose up
q_∞	free stream dynamic pressure
R	propeller radius
S	area of wing panel (free-floating or pinned)
T	propeller thrust
T'_c	propeller thrust coefficient [= $T/A (q_\infty + T/A)$]
AR	aspect ratio

INTRODUCTION

Free-floating tail surfaces were successfully used on the McDonnell XV-1 compound helicopter and on the Convair Charger STOL airplane. Both resulted from a need to operate lifting surfaces in large downwash angle flows. Large downwash angles also occur at the wing location of propeller or rotor V/STOL aircraft at near-hover flight. A case can therefore be made in favor of freeing in pitch the wing panels of these types of aircraft, to let the surfaces weather-vane in the slipstream or rotor wake. This could prevent wing buffet and stall, and would eliminate altogether the hover download problem of tilt-rotor fixed-wing V/STOL aircraft. In case the wing panels remain free during cruise, gust alleviation would be an added benefit. It would also eliminate the need for oversize, and therefore heavy, wing panels, which are presently a feature of tilt-wing V/STOL aircraft. (To prevent buffet and stall during descent and transition, the wing chord must be of the same length as, or larger than, the propeller radius.)

To determine the static aerodynamic characteristics of the free-wing concept, a 1/4-scale powered semispan model (Fig. 1) of a hypothetical five-place 300-knot cruise speed V/STOL airplane was designed and fabricated. The T-tail was omitted from the model. Air inlet and exhaust ports for the twin fuselage-mounted turboshaft engines were faired over in the conventional manner. The model comprises a half-fuselage section mounted on its side, a weather-vaning solid aluminum wing, and a tilting, podded propeller connected through the wing to the fuselage. The trailing edge tab is used to change the wing angle, to increase or decrease lift for wing-panel angle-of-attack control. In the actual airplane the tab would be connected to the pilot's stick. Roll control in cruise would be with differential tab movements, and in hover

Contrails

with differential propeller thrust. Flight path control (climb, descent) in cruise would employ symmetrical tab deflection. During transition the tabs would remain at the up (negative) deflection angle for maximum usable lift coefficient in order to off-load the prop/rotors. The horizontal T-tail surface would serve to counteract the destabilizing pitching moments of the fuselage and propellers, and would be used for trimming the fuselage to a horizontal attitude. A flap and a leading-edge slat are included on the model, although possibly not required on the flight vehicle. Note that the model has a nacelle, while the flight vehicle has none.

TEST FACILITIES

The model was tested in two wind tunnels, namely, the Ling Temco Vought (LTV) 15 x 20' and the U. S. Army Aeronautical Research Laboratory (AARL) 7 x 10' facilities. The maximum dynamic pressure was 6 lbs/ft² in the LTV tunnel, while up to 20 lbs/ft² was utilized in the AARL tunnel.

The LTV tunnel test section contains a moving ground plane which is flush-mounted in the floor. The model was located on the floor just aft of this plane. The moving ground plane was used for every data run, and was set to a speed corresponding to the test free stream velocity. In the AARL tunnel the model was mounted just above a stationary ground board which extended approximately 5 feet ahead of the fuselage nose, and was raised 12 inches above the floor.

MODEL

Two strain-gage-type internal balances were used to measure the loads generated by the propeller and the wing separately. A third strain-gage balance was located inside the fuselage to measure the loads on the entire model assembly. The readings of this balance are not reported here. They are not considered to be representative of a full-span model, due to

the fuselage not being sealed to the floor of the tunnel. Tufts on the floor indicated a strong upwash airflow normal to the fuselage between the fuselage and the tunnel floor even though the average gap was quite small (of the order of $1/4''$). A photograph of the tunnel installation is shown in Fig. 2. The airfoil sections tested are given in Fig. 3.

The model was supported by a block and base plate (Fig. 4), which was bolted to the floor of the LTV $15 \times 20'$ test section, and bolted to the below-floor balance beams of the AARL $7 \times 10'$ test section. The nacelle/propeller assembly was fastened to a hollow shaft (Fig. 4a), which was attached to the model support block. The nacelle contained a 20-hp, aircooled, electric motor, which was coupled to a five-component strain gage balance located between the motor and the propeller. A 3.5-ft. diameter, three-bladed propeller with spinner was fastened to the shaft of the propeller balance. The blades had a constant chord of $1-1/3$ inches, a 14 per cent thick Clark Y section, and 15 degrees of linear spanwise twist. Almost all tests were run at a 6-degree blade angle of incidence measured at the 75 per cent radius station. The instrumentation leads from the motor and balance were routed through the shaft and into the fuselage. The leads then passed under the fuselage and out through the test section floor.

The free-floating wing was attached to an internal balance mounted spanwise inside the wing. The balance was secured by an adapter block which fastened to a hollow wing support shaft (Fig. 4b). The wing shaft was positioned around the nacelle support shaft with a radial clearance of approximately 0.030 inches. The bottom of the shaft contained a ball bearing which fitted into the model support block, and which, in conjunction with a needle bearing at the top, allowed the wing support shaft to rotate freely.

Contrails

The trailing edge of the wing contained a trim tab comprised of three segments. The outboard tab was adjusted manually with brackets prior to each run (δ_3 angle). The center segment was deflected by a remotely controlled electric motor and linkage assembly located inside the wing (δ_2 angle). Tab angles were measured with a potentiometer that was connected to the motor shaft. The inboard tab (δ_1 angle) could be set with brackets, or connected to the center tab (δ_{12} angle) for remote operation. The wing could be locked at fixed incidence angles with a bracket at the base of the support shaft, or allowed to rotate freely during a run. A linear potentiometer was used to record wing angles when in the free-floating mode.

The gaps (of the order of $1/8''$) between the fuselage and the wing and between the wing and the nacelle were unsealed.

The model was tested in both the powered and unpowered configurations. For the unpowered runs the propeller blades only were removed. Each data run consisted of varying the wing tab deflection through a range of angles while holding the test dynamic pressure and propeller thrust constant. Adapter blocks were provided so that the wing could pivot about either the 22% chord or 24% chord position of the basic wing. In the LTV tunnel a pivot at 19.8% chord was also tested by using the 22% chord adapter block and adding a full-span one-inch-wide sheet metal extension to the trailing edge of the basic wing (Fig. 3). For the tests in the AARL tunnel new tabs had been fabricated (extending 1" aft of the trailing edge of the basic wing). For the runs with the flap down and leading-edge slat extended, a 1/2-inch sheet metal extension was added to these new tabs. In the AARL tests the 24% chord adapter block only was used.

The nacelle incidence was varied manually in 15-degree increments

by rotating the main balance support block on the base plate. After rotating the support block the fuselage was repositioned to zero angle of attack. The fuselage was therefore at zero angle of attack for all data runs.

The propeller rpm was measured with an electronic counter at each data point.

A small vane was mounted on the test section floor at the rear of the model to measure tail downwash angles. The vane shaft was connected to a potentiometer for remote read-out.

RESULTS AND DISCUSSION

The model was tested in two different wind tunnels because of anticipated flow breakdown at large propeller tilt angles in the AARL tunnel (propeller/test section area too large), and because of low Reynolds number in the LTV tunnel (maximum $q_{\infty} = 6 \text{ lbs/ft}^2$). The original plan called for model shakedown and cruise tests at AARL, followed by transitional tests at LTV. Due to AARL tunnel unavailability these tests were interchanged. In the following pages the results obtained are presented in the order run, i. e., first the LTV transition data (flap and slat retracted), then the AARL data (flap and slat retracted, and extended). Proper optimization of flap and slat gaps was not possible in the time available in the LTV tunnel. Hence, no data from this tunnel are given for the flap and slat extended case. Gap tuning was subsequently accomplished in the AARL tunnel. No tunnel wall corrections have been applied to the data. In general the LTV data are of better quality than the AARL data.

The AARL data points show considerably more scatter. This might possibly be due to the installation with the fixed ground board in the AARL tunnel. All drag data obtained at AARL are suspect, since many points with negative drag were recorded.

From tuft observations on the upper surface of the wing and from analysis of the data, it is clear that any flight article with a free wing will require a fuselage-to-wing seal to prevent leakage of air through the gap, and thus obtain higher maximum lift coefficients and larger lift curve slopes. The ruinous effect of even small gaps is predicted theoretically in, for instance, Refs. 1 and 2.

It was noted that the free wing responded without apparent lag and without overshoot to changing tab deflection angles. Although the aerodynamic damping in pitch could not be measured in these tests, preliminary in-house tests with a dynamically similar wing and rapid tab deflections confirm a theoretical calculation showing satisfactory damping. A hydraulic rotary damping mechanism for the wing, located on top of the nacelle support block inside the fuselage (see Fig. 4) was never used.

Full-scale propeller disc loading was about 13 lbs/ft^2 . This disc loading was not simulated by the model. Maximum propeller thrust recorded in either tunnel was of the order of 40 lbs, which corresponds to a model disc loading of 4 lbs/ft^2 . All test data have been presented on the basis of T_c'' and α_p .

The wind tunnel tests showed that the trailing-edge angle of the airfoil section had a very large influence on aerodynamic center (a. c.) location. This has previously been noted by other investigators⁽³⁾.

Contrails

It was found that the basic 63 series wing, which according to the data of Ref. 4 should have had the a. c. at 0.27 c, in fact was neutrally stable with the pivot at 0.24 c. A change to the 0.22 c adapter block (2% static margin for the pinned wing) gave the lift curve for the free wing shown on the left in Fig. 5. The corresponding control tab deflection angle is shown on the right. It is seen that the full range of usable positive lift coefficients is obtained with only 5 degrees of tab deflection angle. The same figure also gives the drag polar, which shows a very high zero lift drag. It would have been possible at this point to desensitize the control tab by disconnecting tab 1 and making this a fixed tab, i. e., using tab 2 only for control (see Fig. 1). Instead, it was decided to decrease the trailing-edge angle of the airfoil section by adding a 1" sheet metal extension to the trailing edge (Fig. 3). This modification moved the a. c. rearwards to the 0.26 c position for a gain of 2% in a. c. location as a result of the sharp trailing edge. The same wing pivot was now located at 0.198 c for a 6% static margin of the pinned wing (c being the new chord length). The effect of this modification on the free-wing lift, tab angle for trim, and drag is given in Fig. 5. A large gain is shown in zero lift drag. Maximum lift is somewhat decreased. It now takes a more reasonable 15 degrees of tab angle to trim the full range of usable positive lift coefficients. This improved configuration was subsequently tested in the LTV tunnel over the full range of T_c'' and α_p . The results are presented in Figs. 6-12.

From Fig. 6 (cruise condition) it is apparent that the lift curve

slope wing-pinned is 0.074/degree, which corresponds to $ARe = 4.17$. The geometric aspect ratio of the wing panel is 2.37. The gapped wing therefore behaves aerodynamically as if it had double the span, approximately. The maximum lift coefficient wing-free is around 0.9 at the test Reynolds number of 350 000. It is noted that the drag increase due to free floating the wing is quite low at cruise lift coefficients ($\bar{C}_L \approx 0.4$). Thus the penalty for trimming the wing with a trailing-edge tab, rather than with an aft tail surface, is low. It is also seen that the recorded pitching moments of the free wing around the pivot (theoretically zero) are very low, indicating low friction in the bearings.

At very high transitional speeds (Fig. 7) the lift curve slope is already considerably lower than at cruise. The maximum lift coefficient is decreased to around 0.7 - 0.8. The same trend would, of course, be obtained for a fixed wing. The control tab angle for trim is essentially unchanged as compared to Fig. 6. Rather remarkable in Fig. 7 is the higher lift coefficient recorded for $\alpha_p = 15^\circ$ than for $\alpha_p = 0$; i. e., for T_c'' held constant the wing experiences an upwash, rather than a downwash as would have been expected. It is believed that higher propeller swirl at $\alpha_p = 15^\circ$ (the propeller rotates up inboard), upwash created by the rotated nacelle, and upwash outside the slipstream by the wing root at $\alpha_p = 15^\circ$ interact with the downwash created by the deflected slipstream to result in a net upwash component.

The identical trend is evident at higher T_c'' (Figs. 8 and 9). A reversal of the trend is starting in Fig. 10, and in Fig. 11 the data show a slight downwash angle being recorded in passing from $\alpha_p = 45^\circ$ to $\alpha_p = 60^\circ$. It is somewhat surprising that even at $T_c'' = 0.66$ and $\alpha_p = 60^\circ$ (Fig. 11) the slipstream does not turn the flow significantly. The wing still operates as if it were in a parallel stream from infinity (the wing angles of attack are between 0° and 20°).

However, in Fig. 12 ($T_c'' = 0.84$, $\alpha_p = 75^\circ$) the slipstream turning is evident. Here the wing is operating at around 30° angle of attack. Data at the lower angles of attack could not be obtained due to the wing bottoming out against a stop.

In reviewing Figs. 6 - 12, it is noted that the slope of the lift curve decreases progressively as T_c'' is increased. This is in accordance with established theory⁽⁵⁾, since at static conditions ($T_c'' = 1$) the lift curve slope is predicted to be only 60 per cent of its value at cruise ($T_c'' \approx 0$). The maximum lift coefficients exhibit a similar decreasing trend with increasing T_c'' . It is seen that the tab angles to trim remain fairly constant; nor is there much change in the slope $d\bar{C}_L/d\delta_{12}$.

The model was next tested in the AARL tunnel. A comparison of the lift curves in the two tunnels is given in Fig. 13. It is seen that the difference is quite small at zero lift. The fact that the slopes are different might be ascribed to a slight change in the wing/fuselage gap. The gap was possibly smaller for the AARL tests. This might also explain the very large decrease in drag due to lift in the AARL tests (see Fig. 14 as compared to Fig. 6). Figure 14 indicates that the cruise static margin wing-pinned at

Contrails

AARL is 4% (as compared to 6% for the LTV tests), which is consistent with the use of the 0.24 c adapter block and the one-inch extended chord (T. E. 3).

With the lower static margin it was decided to use the center tab (δ_2) only for control. Figure 15 shows that the static margin wing-pinned at $\alpha_p = 45^\circ$ and $T_c'' \approx 0.55$ is slightly increased from that at cruise (6% versus 4%).

At low lift coefficients there seems to be a destabilizing trend. No instabilities were, however, observed for this configuration with the wing free at any lift coefficients.

Superimposed upon the wing-pinned data of Fig. 14 is a wing-free data run which does not correspond to the wing-pinned data, since the thrust coefficients are different. The $T_c'' = 0$ wing-free data, which would have corresponded, were lost by the tunnel operating personnel. The heavy lines of Fig. 14 ($\alpha_p = 0$) should be compared with the $\alpha_p = 15^\circ$ data in Fig. 8 for the same thrust coefficient, but with different static margin and control tab span. It is noted that the lift curve slope is steeper for the configuration with the lower static margin, the maximum lift coefficient is higher, and $d\bar{C}_L/d\delta$ is the same for both tab spans.

Figures 16 and 17 for, respectively, $\alpha_p = 30^\circ$ and 60° show the results obtained by keeping propeller angle of tilt constant and varying the thrust coefficient. As was evident from the LTV data, both the lift curve slope and the maximum lift coefficient decrease with increasing T_c'' . There is no apparent indication that the slipstream has turned the free-stream flow.

So far, all test results reported have been for the flap and slat retracted case. Flap and slat extended data are presented in Figs. 18 and 19. A 1/2" sheet metal extension was added to the wing trailing edge in an attempt to cure a slight instability at small negative angles of attack. This instability

showed up as a slow movement of the wing to a negatively stalled condition without additional control tab deflections after a slightly negative angle had been reached. The trailing edge extension did not, however, measurably improve this condition. Additional tests are required to understand and then remove the instability. The instability is not apparent from the wing-pinned moment curve in Fig. 18 (δ_{12} positive). This curve shows a 7.7% static margin based upon the extended chord (11% based upon the retracted chord), a value which is considered too high. Since the pivot is at approximately $0.22 c_{\text{extended}}$, the a. c. flap and slat extended is located at 29.7%. The aft a. c. location could be caused by the leading-edge slat not carrying its share of the lift due to slightly off-optimum positioning. Due to the excessive static margin the maximum lift coefficient is not more than 1.7 (Fig. 18).

For some reason, the static margin must be much reduced at $\alpha_p = 45^\circ$, since as shown in Fig. 19 the maximum lift coefficient reaches a value of 2.3 at low thrust coefficients, and is equal to 2.0 at $T_c'' \approx 0.25$. With additional testing it should therefore also be possible to reach at least $\bar{C}_L = 2.3$ at $\alpha_p = 0$, $T_c'' \approx 0$.

From the five-component thrust balance, complete information about the propeller forces and moments was obtained. The thrust vector offset distances in pitch have been plotted in Fig. 20 for both flap and slat retracted, and extended, at zero lift coefficient. In general, it appears that slightly less offset is obtained with flap and slat extended. It is noted that the propeller is unstable with respect to angle of attack changes, as is well known. Thrust vector offset distances in the spanwise direction were also determined, but are not presented here.

Contrails

Observations of the oscillations of a small vane, mounted on the tunnel floor at two possible locations of the horizontal tail surface, indicated that a low (conventional) tail position would not be acceptable, because of severe flow disturbances at propeller angles of 60 and 75° power on. With the vane located at the T-tail position, no adverse flow disturbances were observed. Downwash angles were recorded, but are not presented here.

Free-wing tests at $\alpha_p = 90^\circ$ and $T_c'' \approx 1$ were attempted. However, slipstream recirculation, the ground impingement fountain effect, combined with adverse tunnel wall interference resulted in large-scale wing oscillations, and prevented any measurements to be taken. If the free wing should be used for airplane yaw control during take-off and landing, oscillations of this type would be unacceptable. It is suggested that the airplane might be configured to take off and land with 80-85 degrees of propeller tilt (instead of 90°) and with the free wing trimmed at its maximum usable lift coefficient in order to cancel the horizontal component of propeller thrust. Future tests would have to determine if this is feasible. So far, it is known that a small amount of tilt away from the vertical is greatly beneficial in reducing the upstream extent of flow along the ground⁽⁶⁾. No wing oscillations were observed in either the LTV or AARL wind tunnels at $\alpha_p = 75^\circ$ and $T_c'' = 1$ (static condition).

Finally, it might be mentioned that the results presented above represent a summary of the two initial tests only of the free-wing tilt-propeller concept. Other tests will follow on the same basic 1/4-scale model, but with a dynamically similar wing (under a U.S. Army contract).

In retrospect it is felt that additional interesting test results would have been obtained from the model if the wing-fuselage and fuselage-floor gaps had been sealed (weatherstripping or brush seal), and if data could have been taken in the LTV tunnel at intermediate propeller angles of tilt between 75° and 90° at thrust coefficients near unity.

REFERENCES

1. Durand, W. F.: Aerodynamic Theory. Dover Publications. Vol. II, Sec. 20, pp. 212-214.
2. Nielsen, J. N.: Missile Aerodynamics, McGraw-Hill, 1960.
3. Seckel, E.: Stability and Control of Airplanes and Helicopters. Academic Press, 1964, p. 8.
4. Abbott, I.A., and von Doenhoff, A. E.: Theory of Wing Sections. Dover Publications, 1959, p. 184.
5. Strand, T.; Levinsky, E. S., and Wei, M. H. Y.: "Unified Performance Theory for V/STOL Aircraft in Equilibrium Flight." Parts I and II. Journal of Aircraft, March-April and May-June 1967.
6. Abbott, W. A.: "Studies of Flow Fields Created by Vertical and Inclined Jets when Stationary or Moving over a Horizontal Surface." British ARC C.P. No. 911, 1967.

Contrails

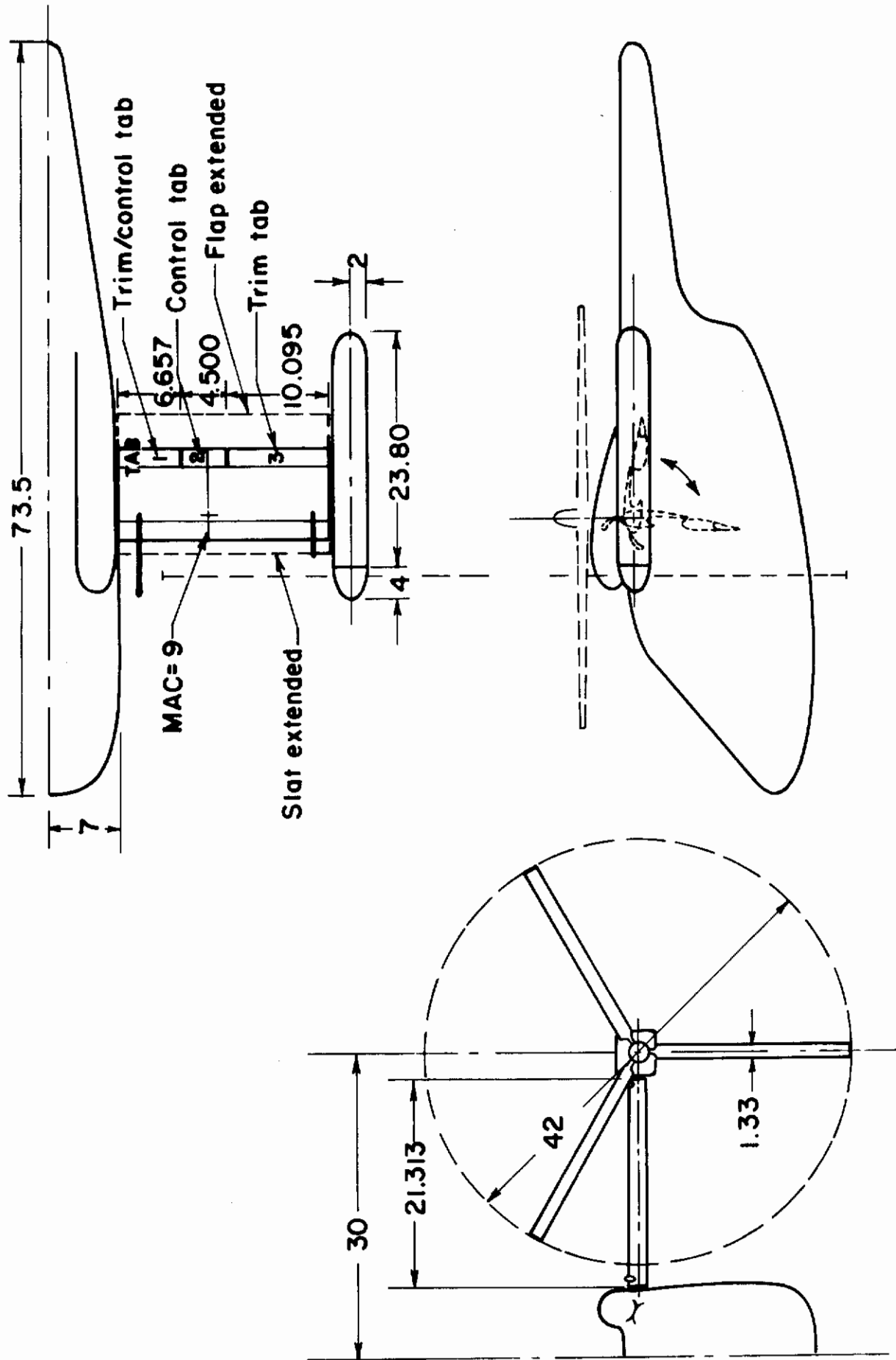


Fig. 1. Three-view of wind tunnel model.

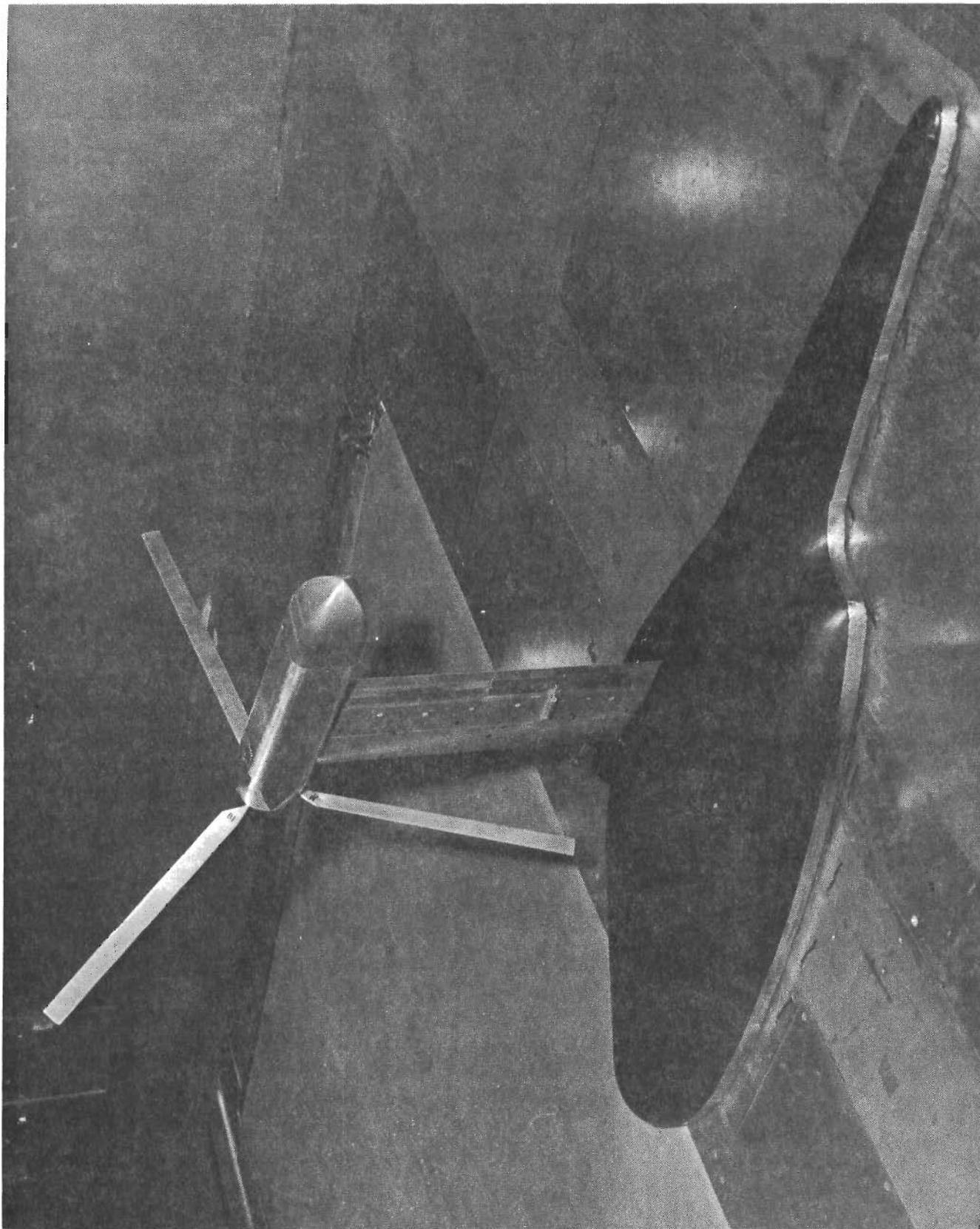


Fig. 2a. Semispan model in the LTV wind tunnel.

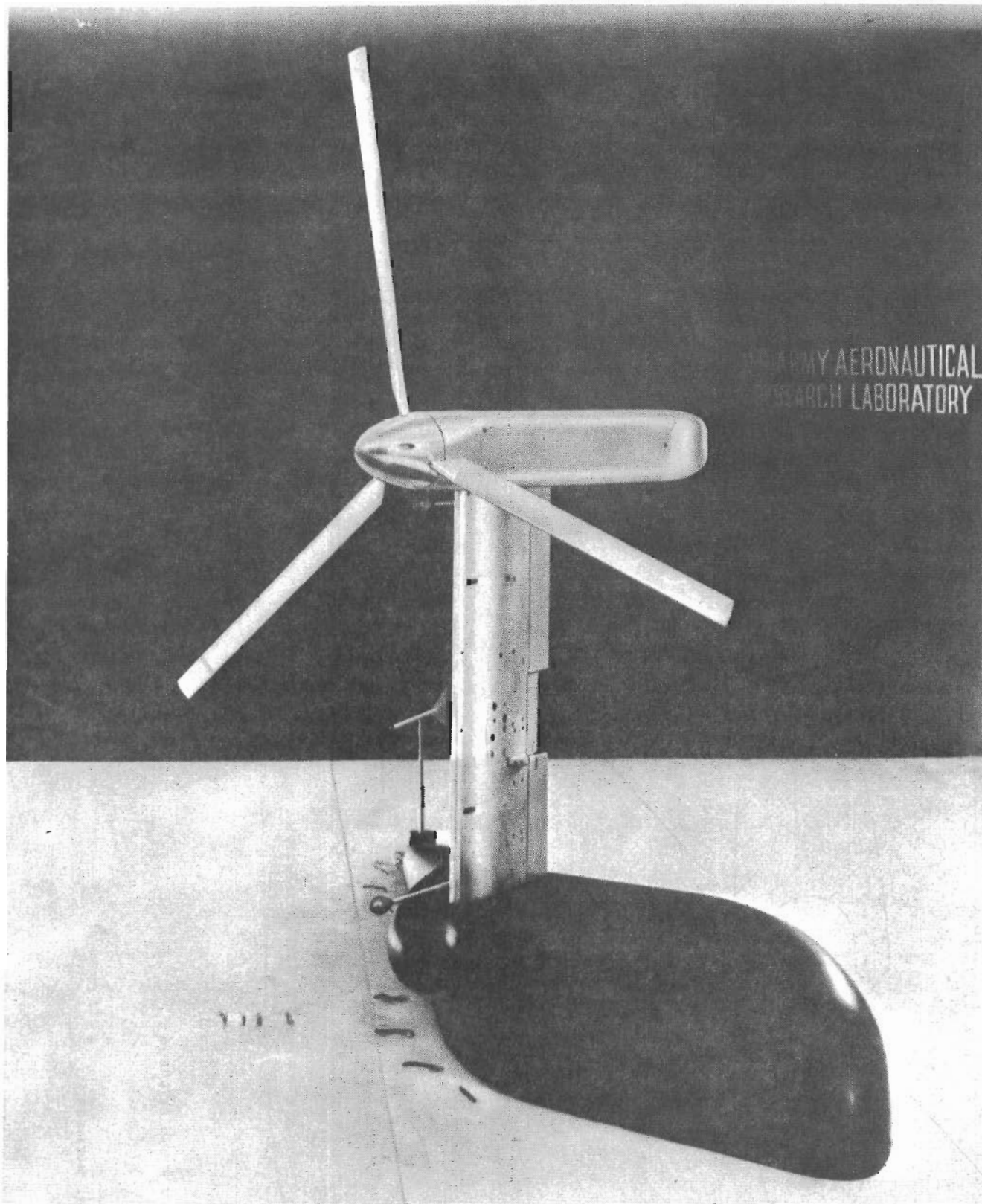


Fig. 2b. Semispan model in the AARL wind tunnel.

Air Vehicle 63₂ A (015) - 219
reflex camber airfoil

x_u/c	y_u/c	x_L/c	y_L/c
0	0	0	0
.002	.016	.008	-.014
.004	.020	.011	-.016
.009	.026	.016	-.021
.021	.037	.029	-.028
.045	.053	.055	-.039
.070	.065	.080	-.046
.095	.075	.105	-.052
.146	.090	.154	-.061
.197	.100	.203	-.067
.248	.108	.252	-.072
.300	.112	.300	-.075
.352	.113	.348	-.077
.403	.110	.397	-.078
.454	.105	.446	-.077
.504	.098	.496	-.075
.555	.090	.545	-.072
.606	.080	.594	-.067
.656	.079	.644	-.062
.706	.058	.694	-.055
.756	.046	.744	-.048
.805	.035	.795	-.040
.855	.026	.845	-.030
.903	.017	.897	-.021
.952	.009	.949	-.011
1.000	.000	1.000	-.000

L.E. radius = 0.186', $\theta = 10.8^\circ$
T.E. radius = 0.004

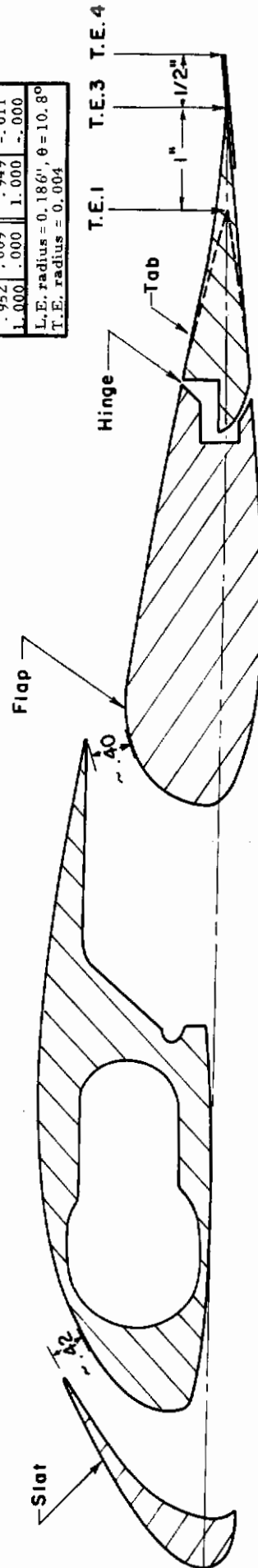
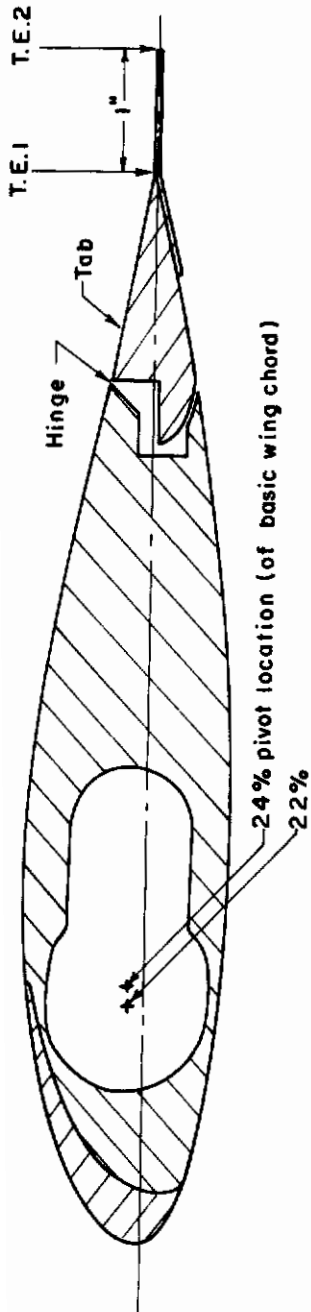


Fig. 3. Airfoil sections.

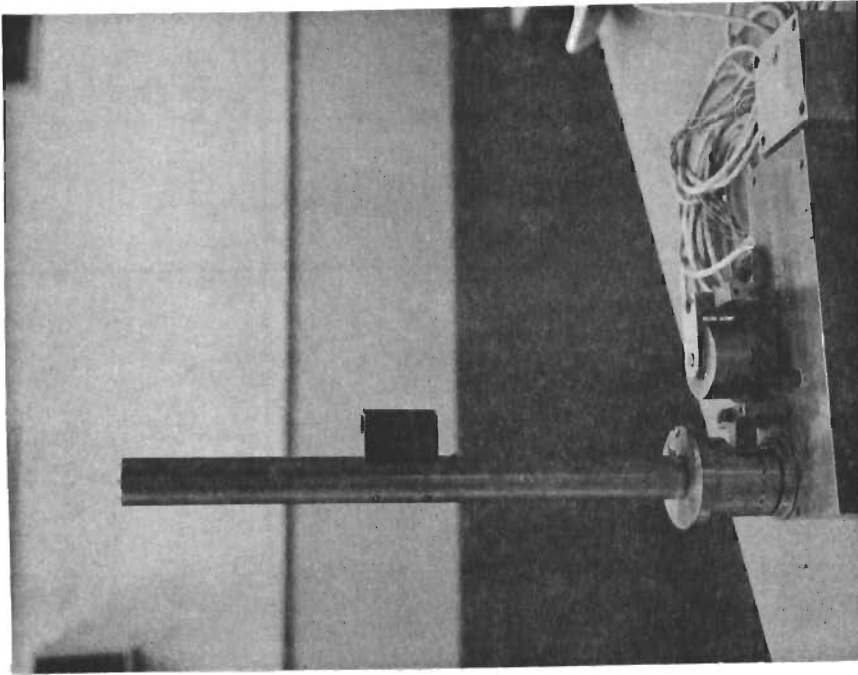


Fig. 4b
Free-wing support shaft

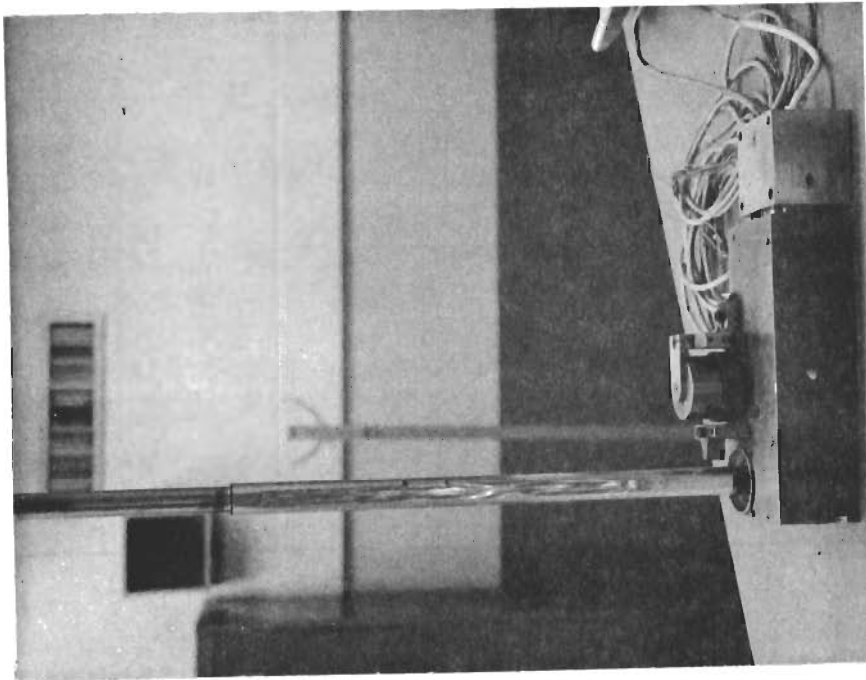


Fig. 4a
Nacelle support shaft

Fig. 4. Model support block, fuselage balance support block, wing oscillation damper assembly (not used), nacelle support shaft, and wing support shaft.

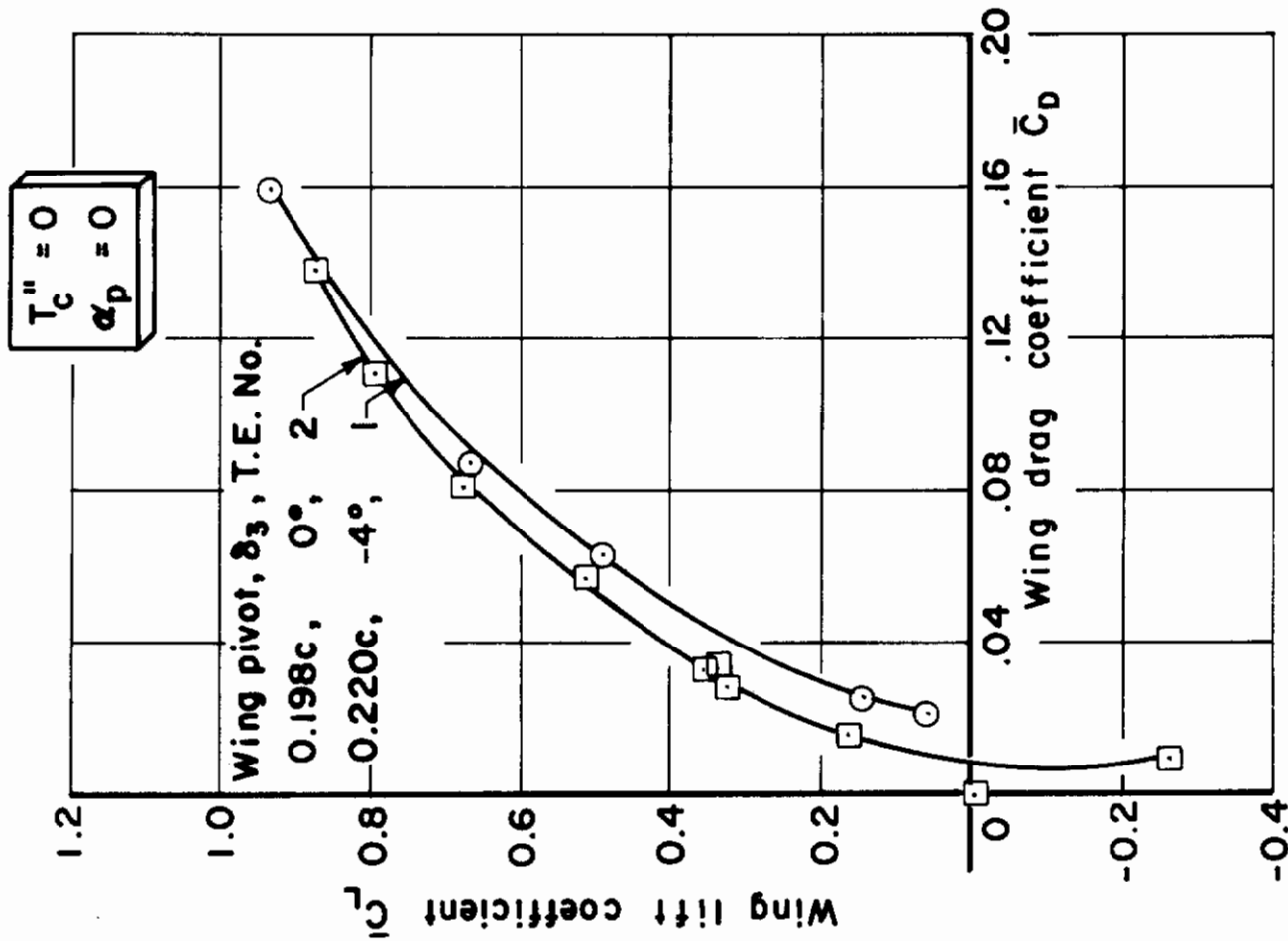


Fig. 5 continued. Effect of pivot location and wing trailing edge angle on drag.

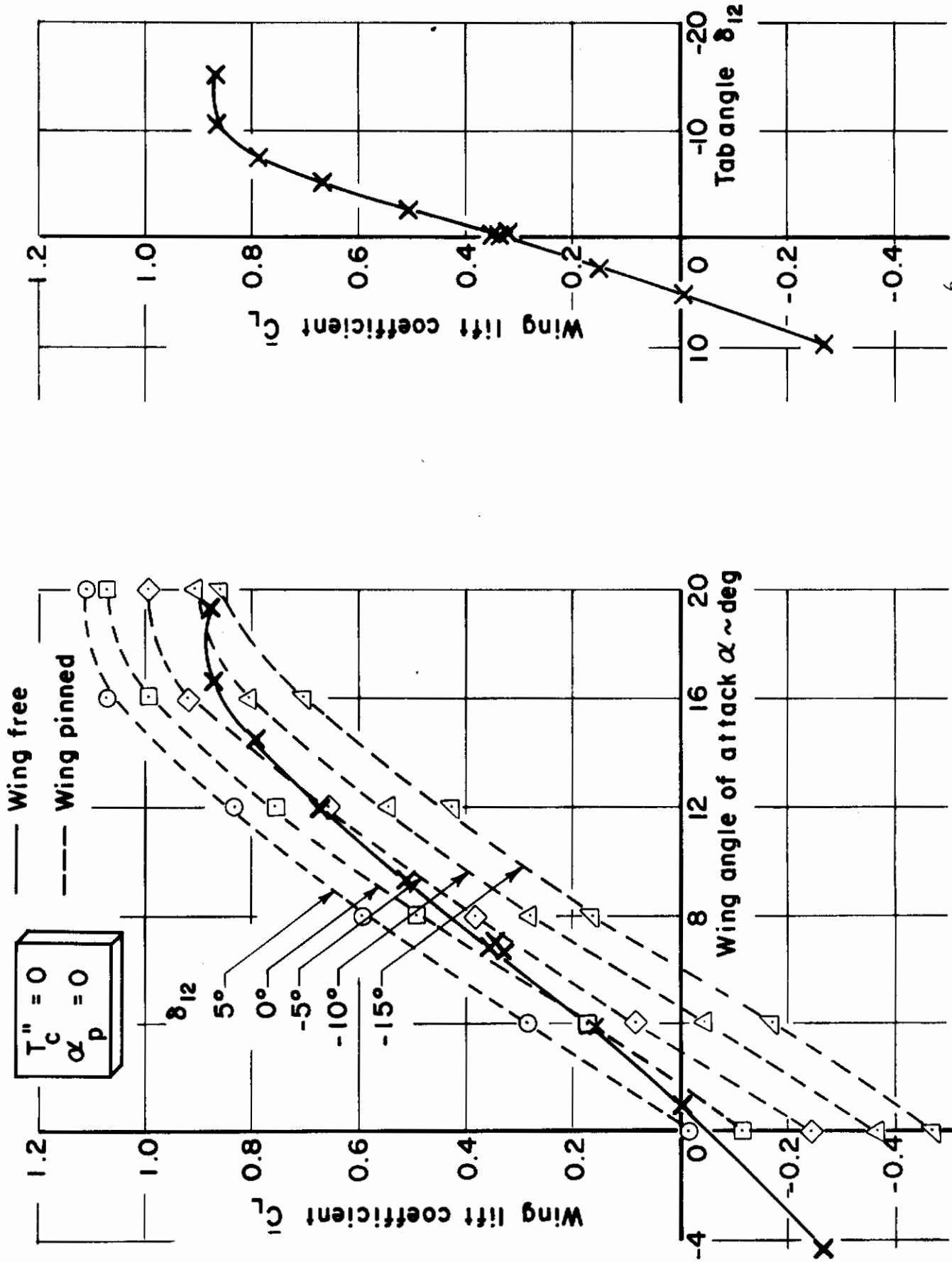


Fig. 6. Lift (flap and slat retracted, propeller off, T. E. 2, $\delta_3 = 0$, $Re \approx 0.35 \cdot 10^6$, pivot at 0.198 c, LTV tunnel, $q_\infty = 6$).

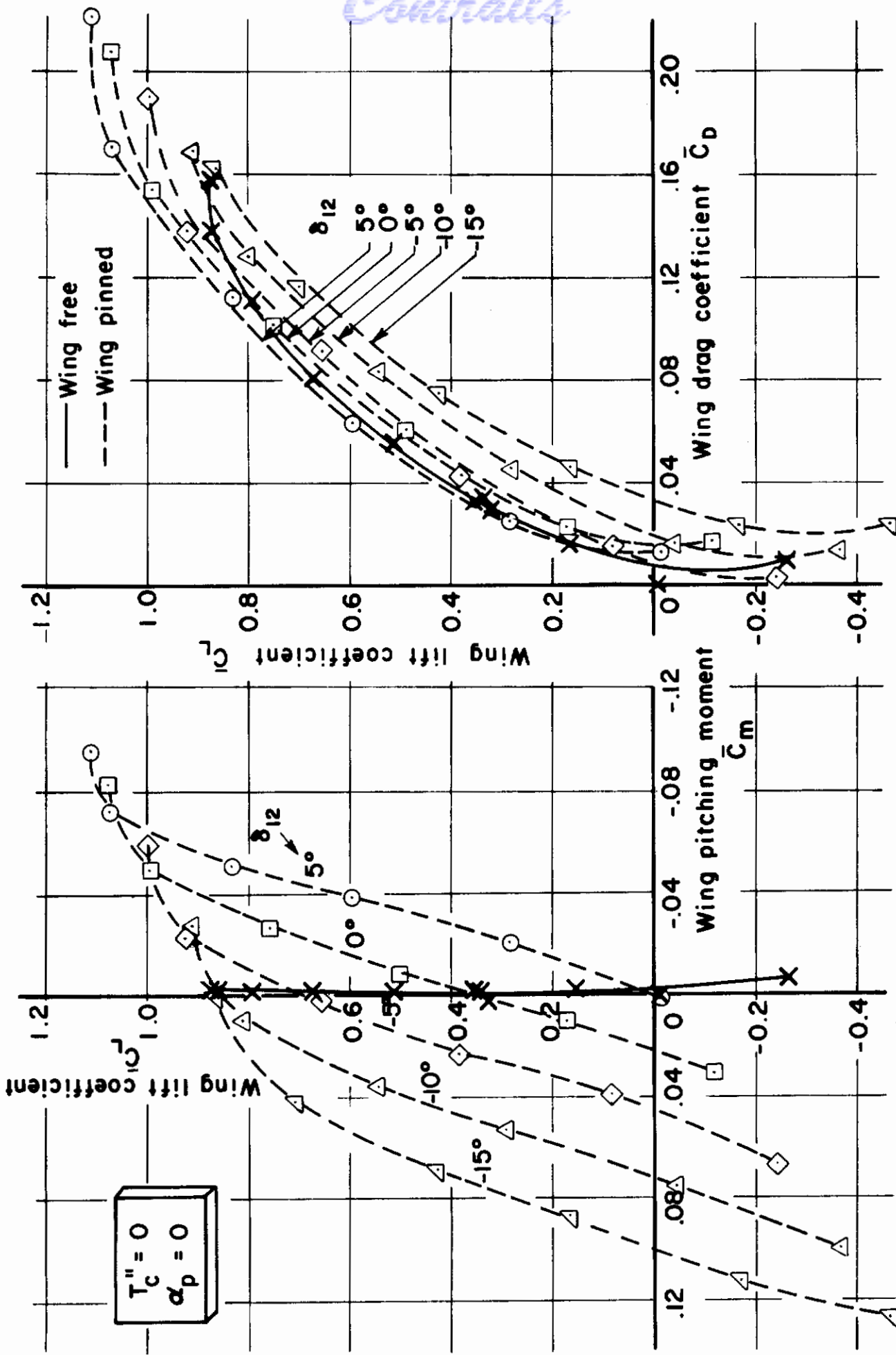


Fig. 6 continued. Pitching moment and drag.

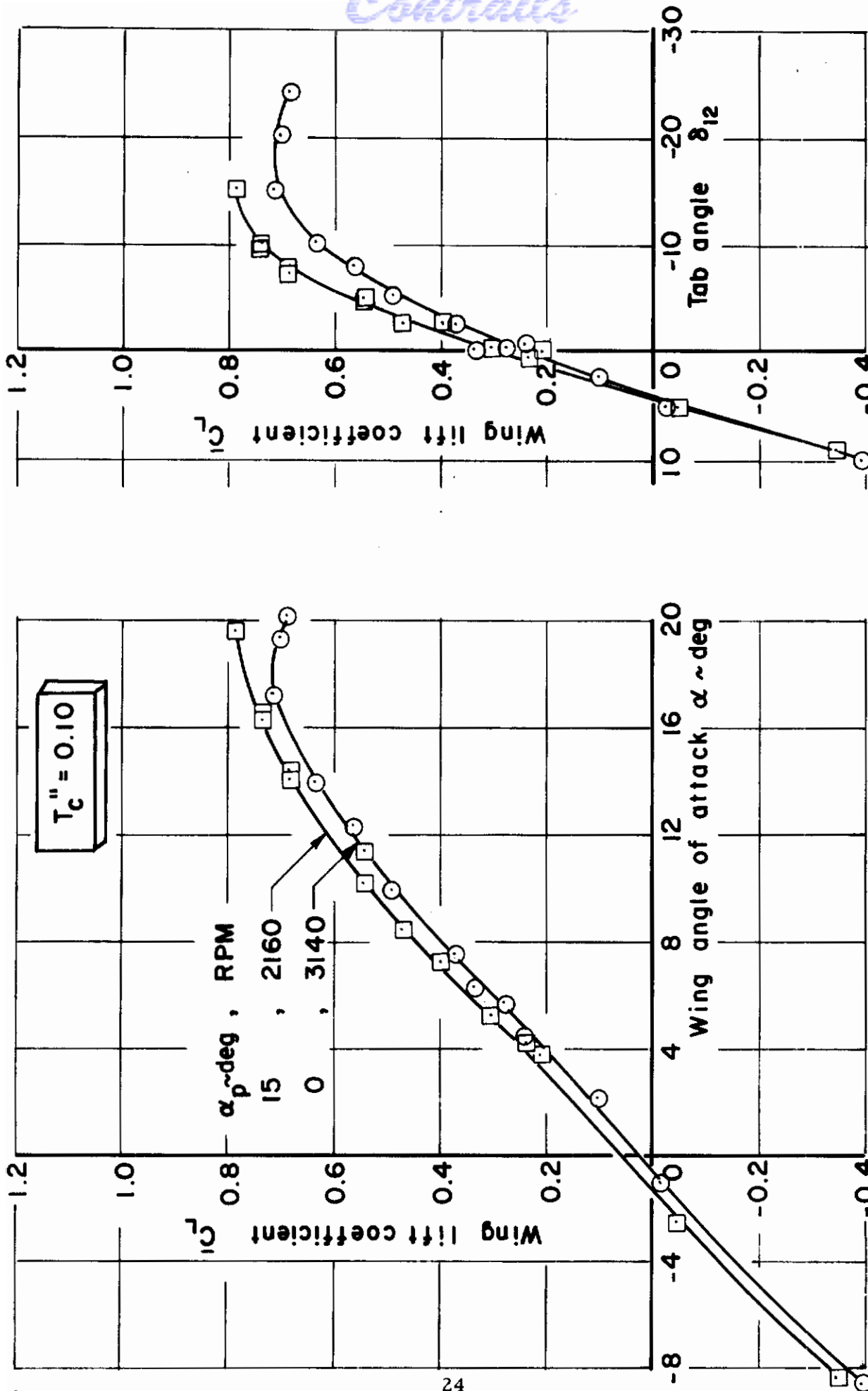


Fig. 7. Lift (wing free, flap and slat retracted, T.E. 2, $\delta_3 = 0$, $Re \approx 0.35 \cdot 10^6$, pivot at 0.198 c, LTV tunnel).

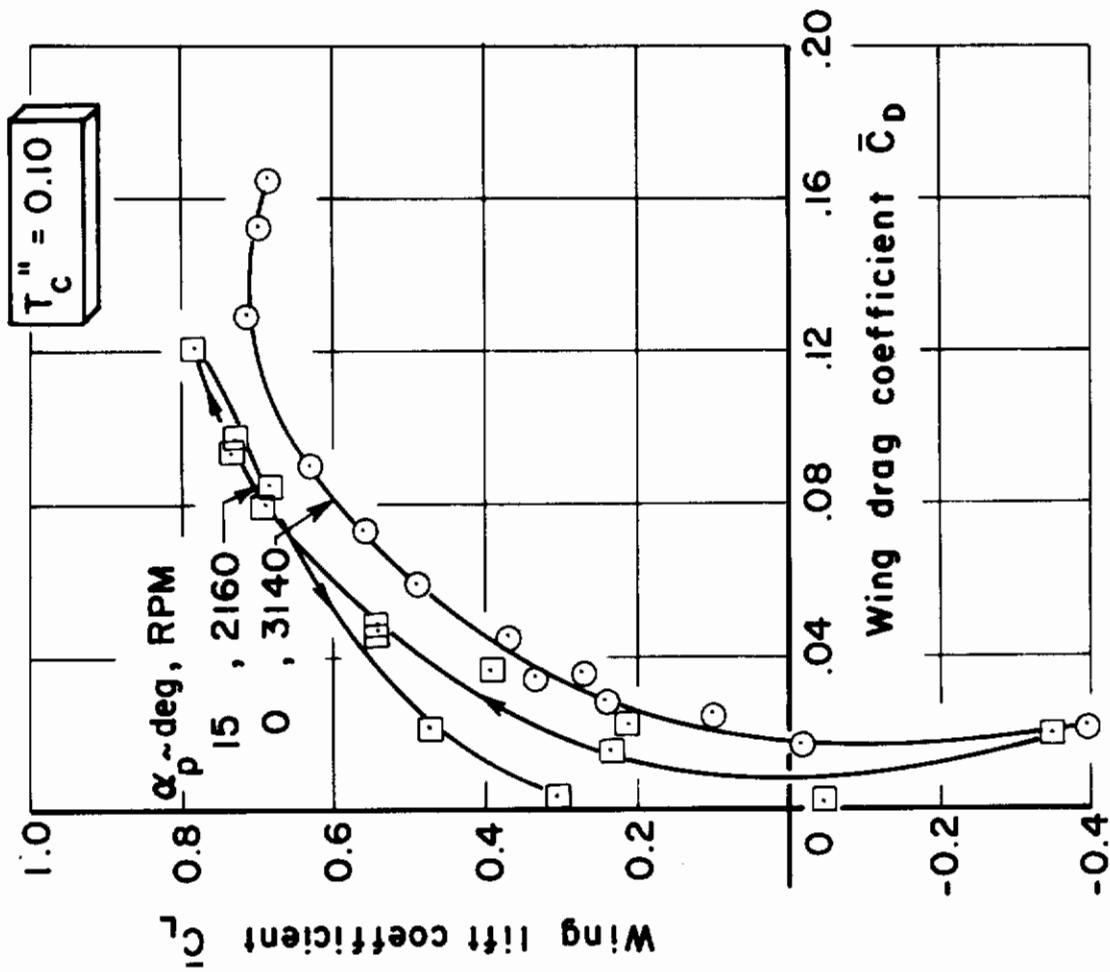


Fig. 7 continued. Drag polars.

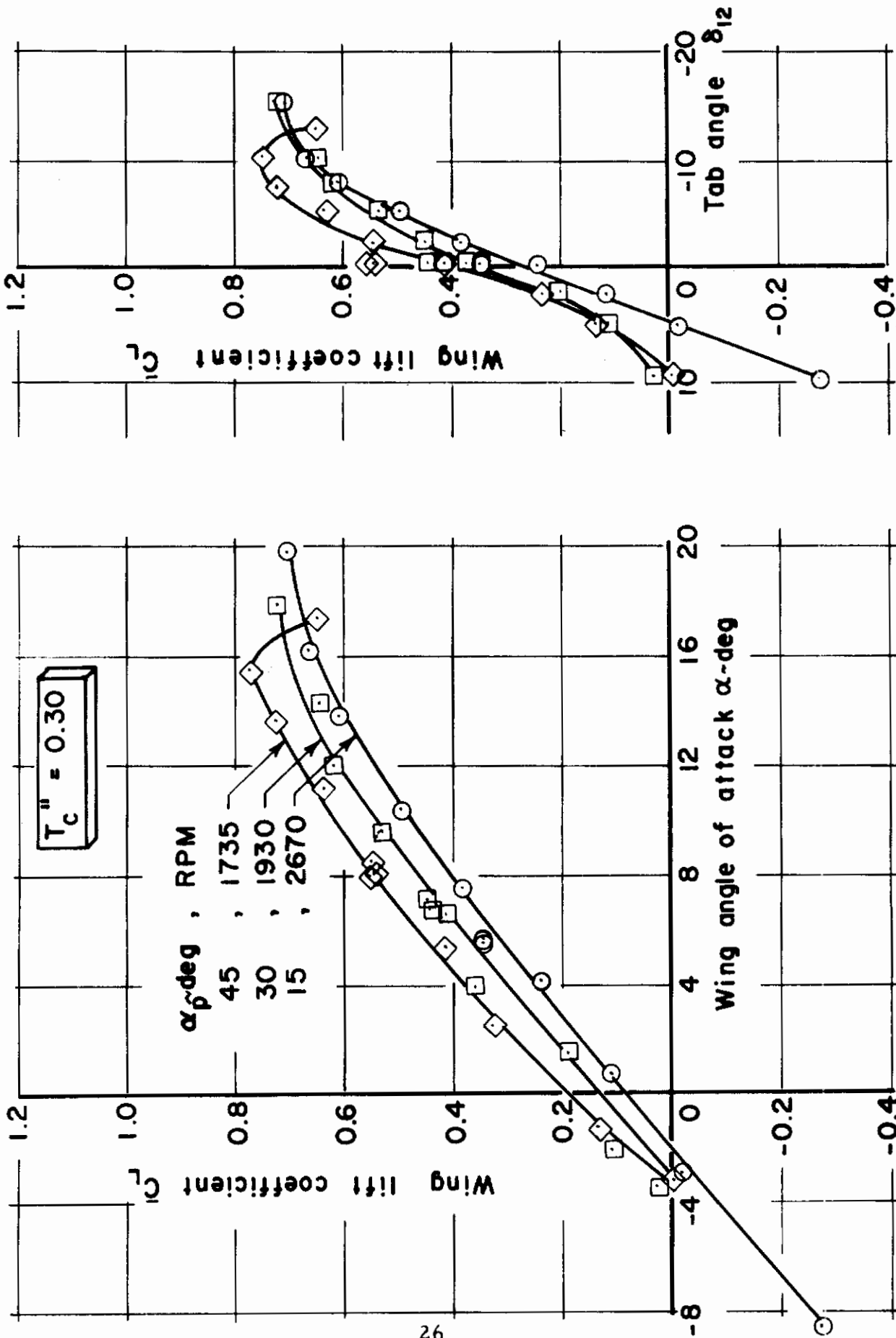


Fig. 8. Lift (wing free, flap and slat retracted, T. E. 2, $\delta_3 = 0$, $Re \approx 0.35 \cdot 10^6$, pivot at 0.198 c, LTV tunnel).

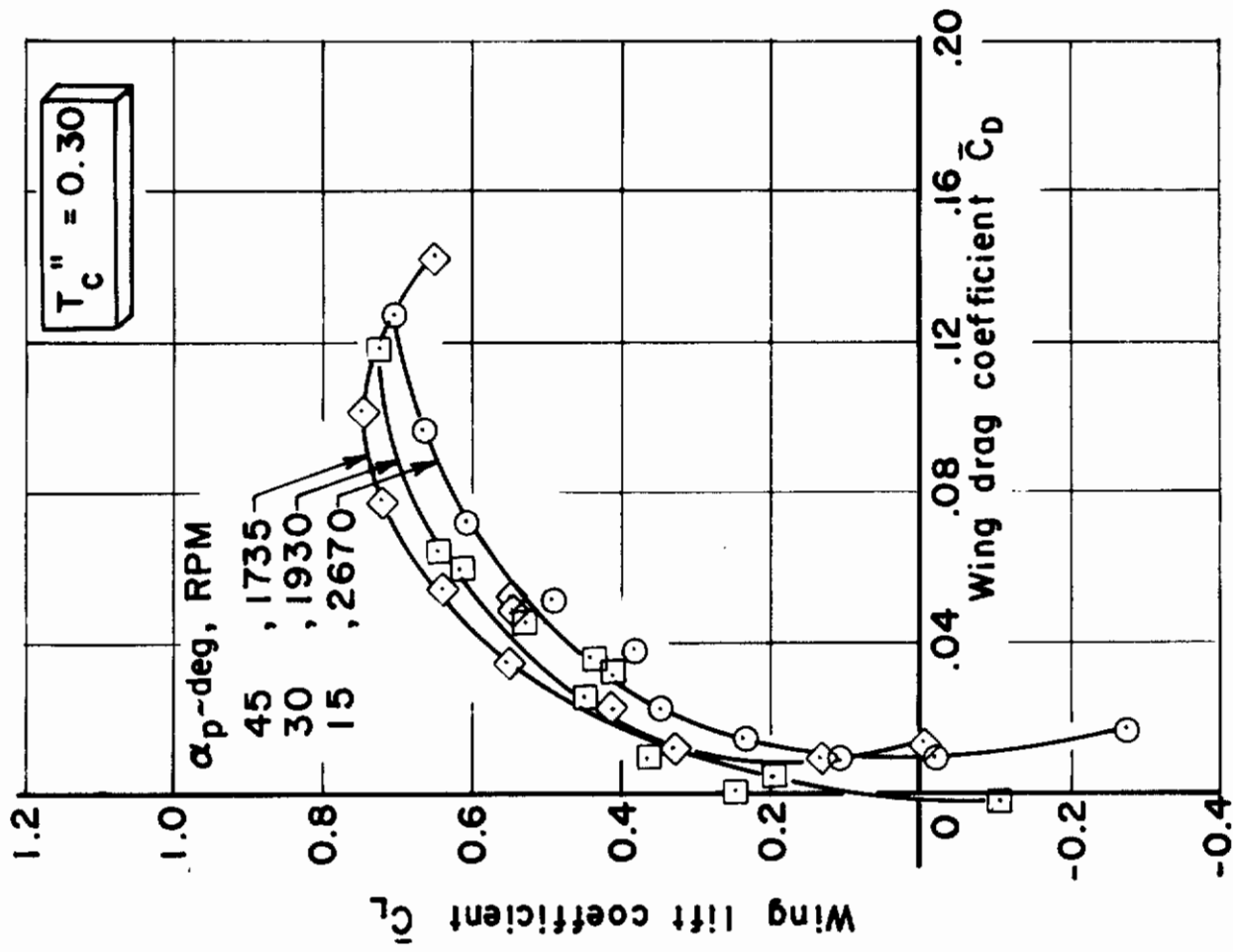


Fig. 8 continued. Drag polars.

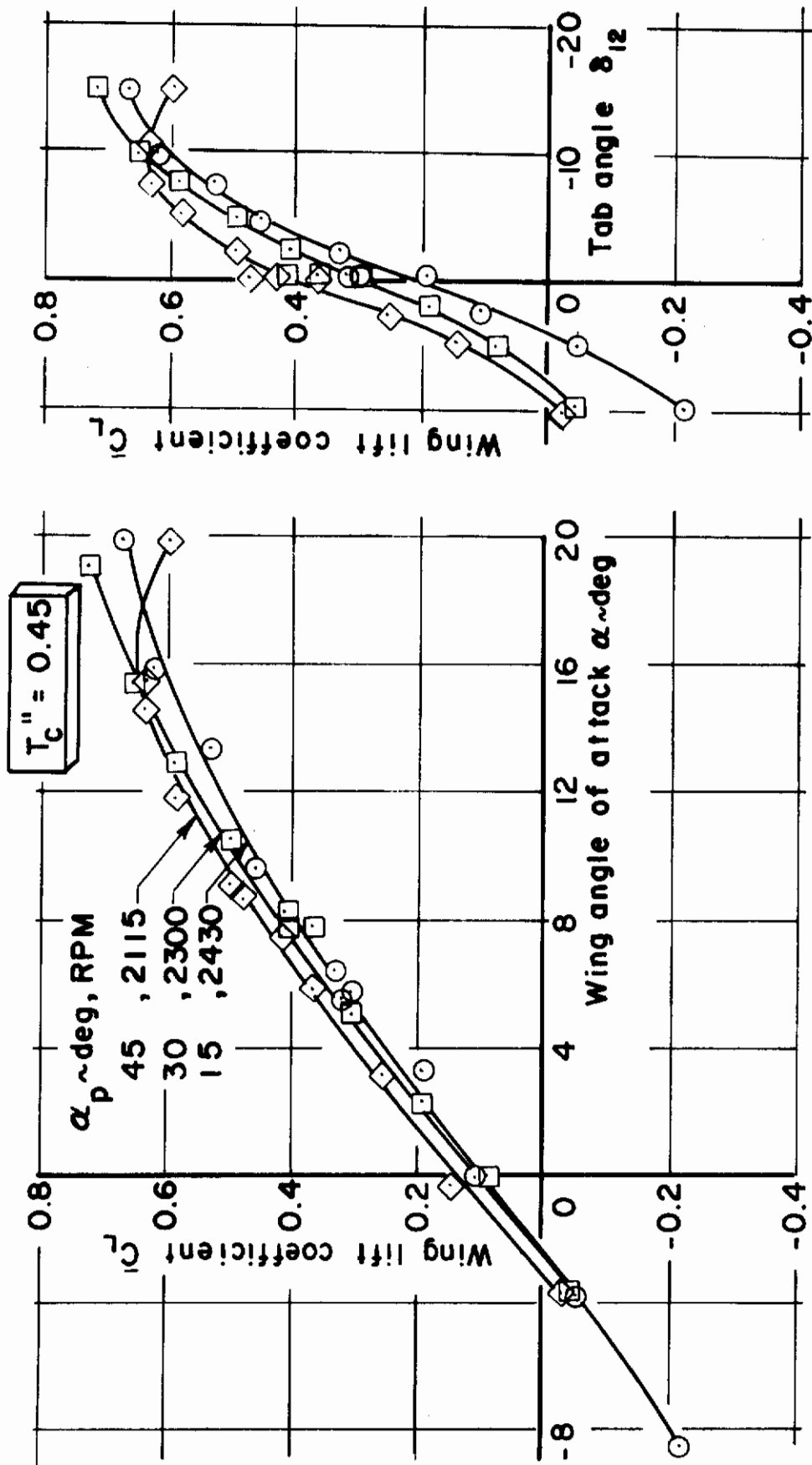


Fig. 9. Lift (wing free, flap and slat retracted, T. E. 2, $\delta_3 = 0$, $Re \approx 0.35 \cdot 10^6$, pivot at $0.198c$, LTV tunnel).

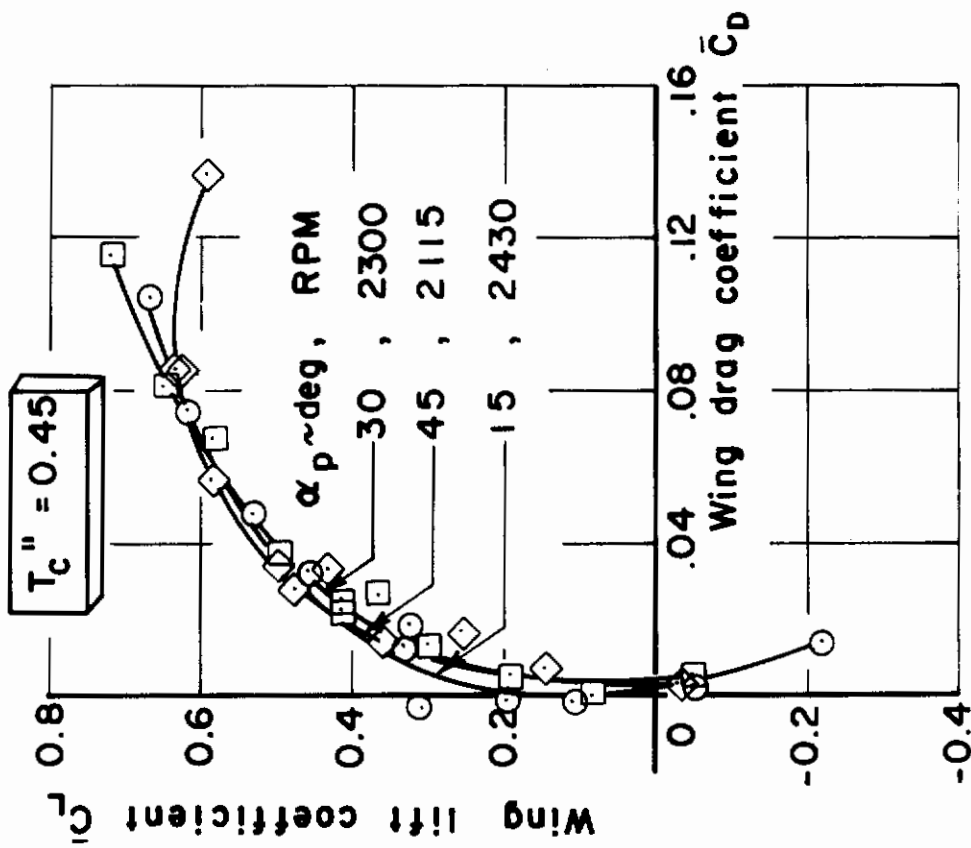


Fig. 9 continued. Drag polars.

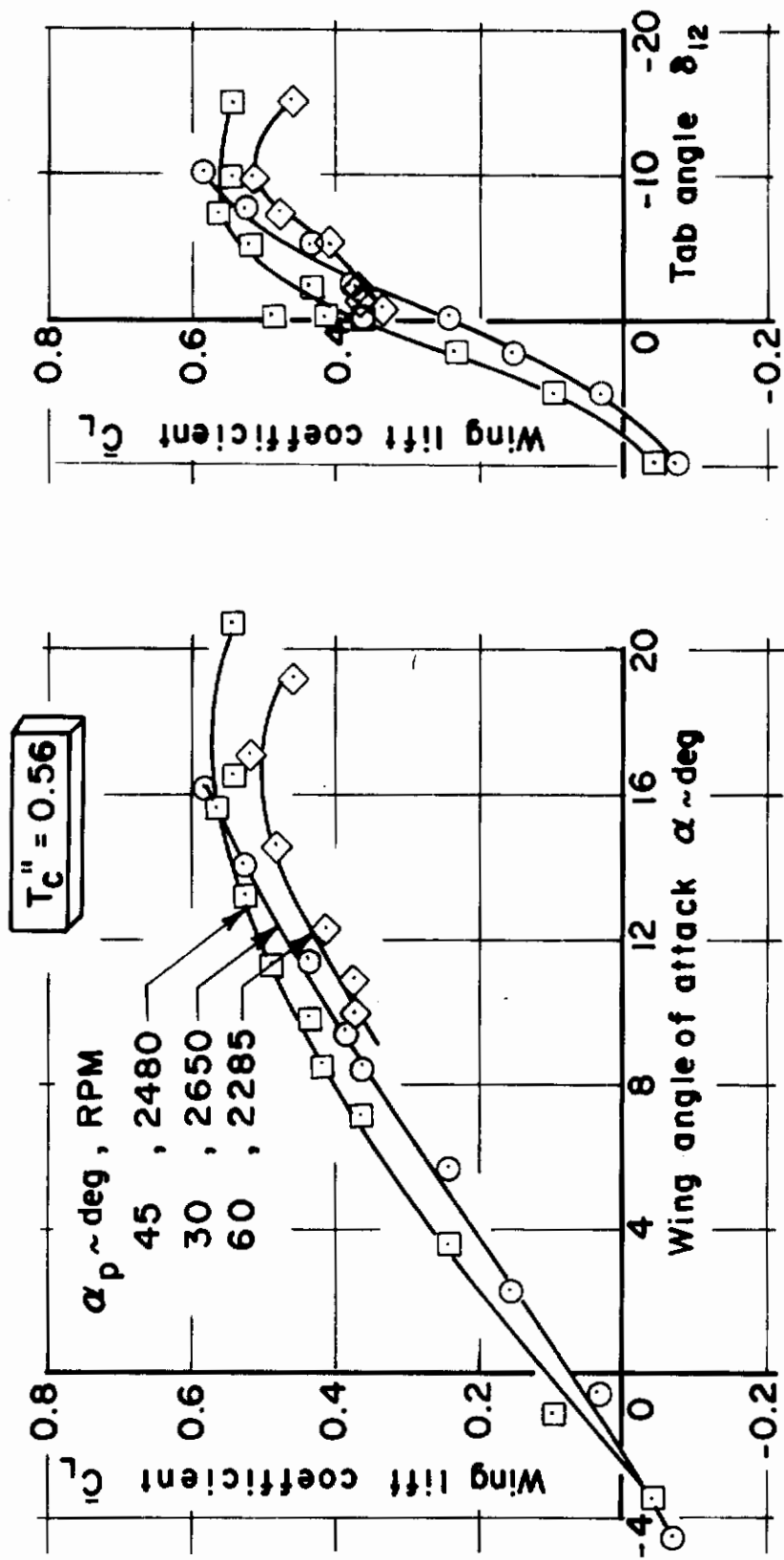


Fig. 10. Lift (wing free, flap and slat retracted, T. E. 2, $\delta_3 = 0$ Re $\approx 0.35 \cdot 10^6$, pivot at 0.198 c, LTV tunnel).

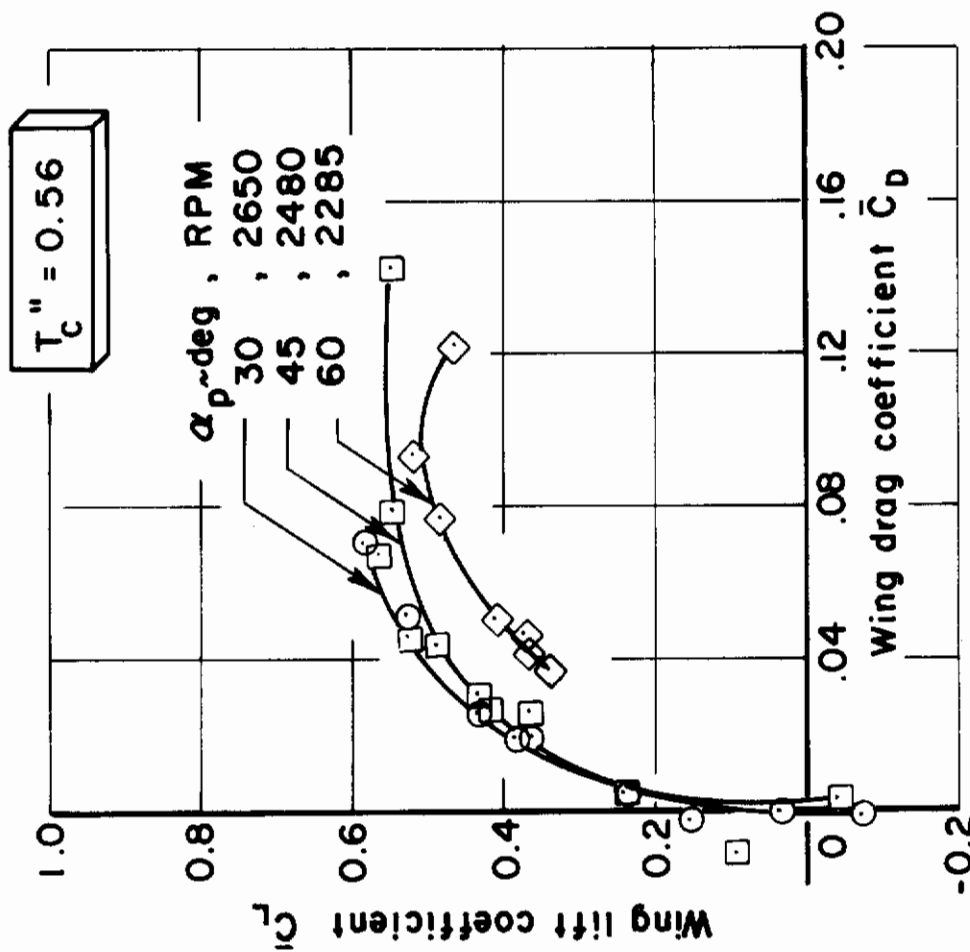


Fig.10 continued. Drag polars.

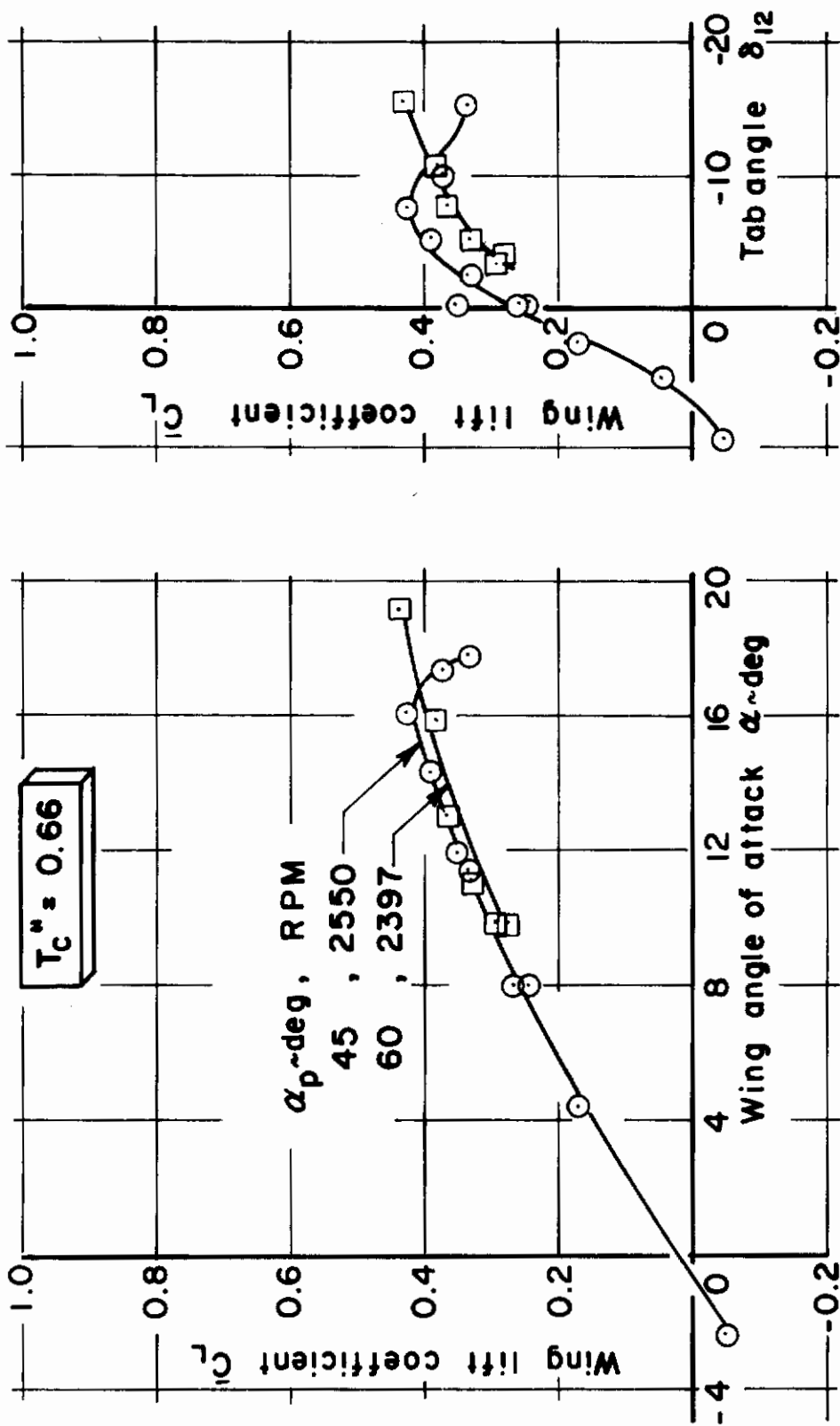


Fig. 11. Lift (wing free, flap and slat retracted, T.E. 2, $\delta_3 = 0$, $Re \approx 0.35 \cdot 10^6$, pivot at $0.198 c$, I,TV tunnel).

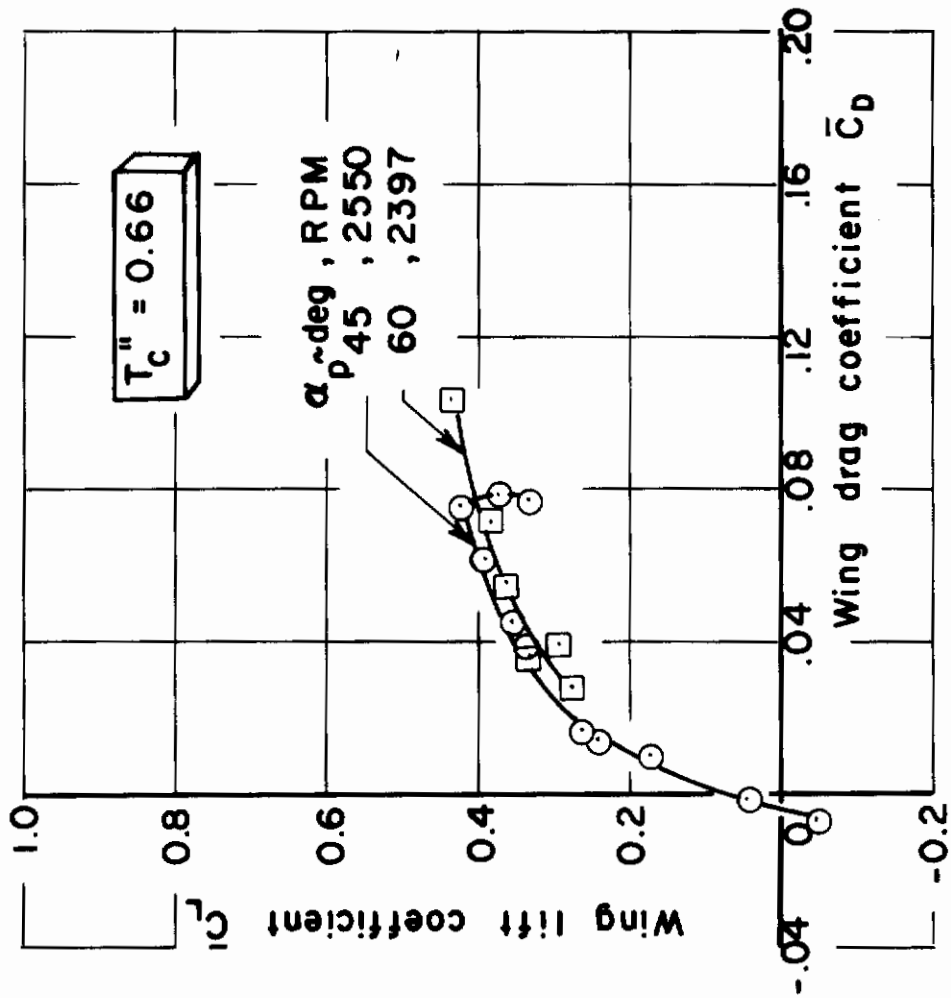


Fig. 11 continued. Drag polars.

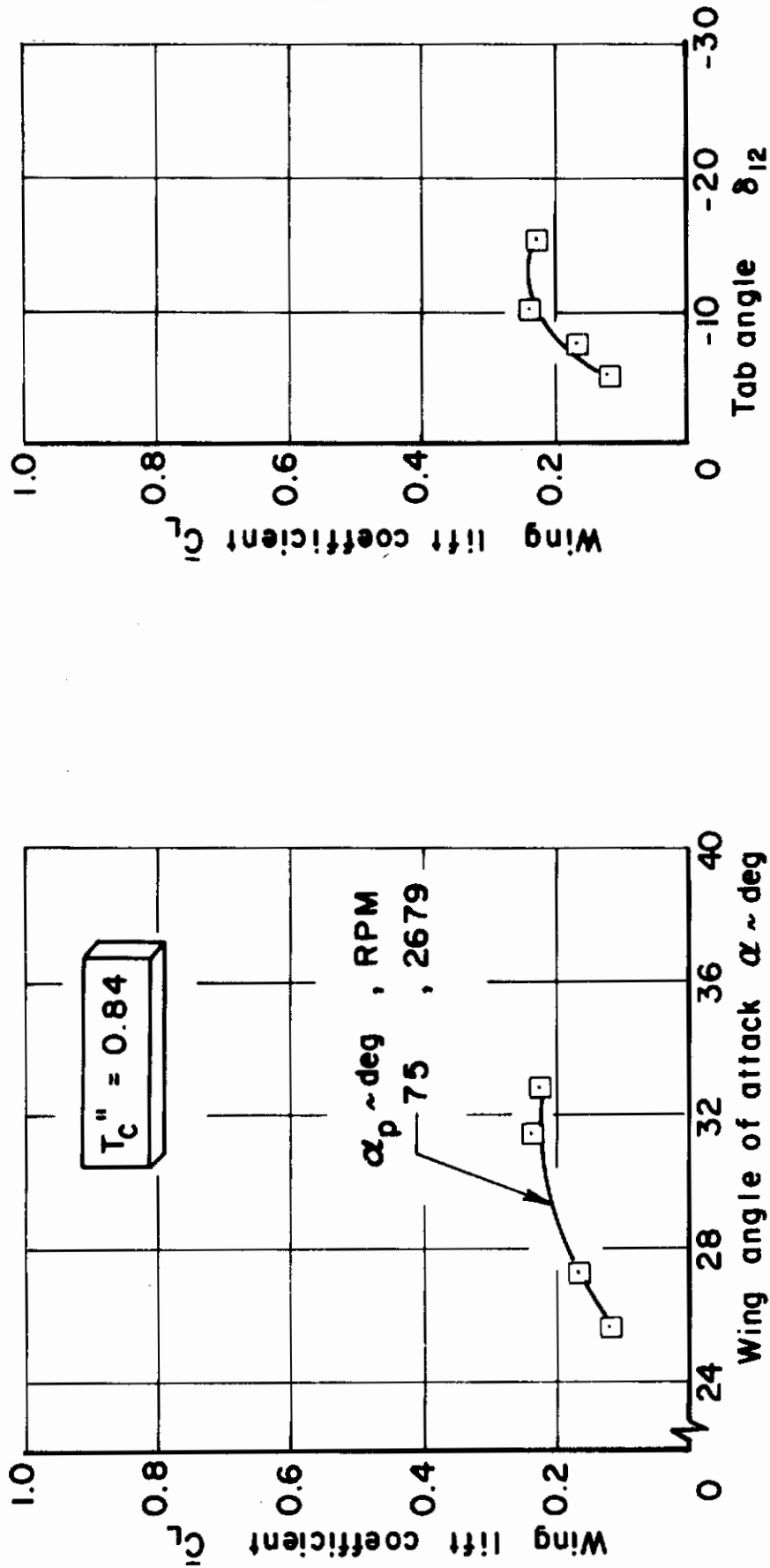


Fig. 12. Lift (wing free, flap and slat retracted, T.E. 2, $\delta_3 = 0$, $Re \approx 0.35 \cdot 10^{-6}$, pivot at $0.198c$, LTV tunnel).

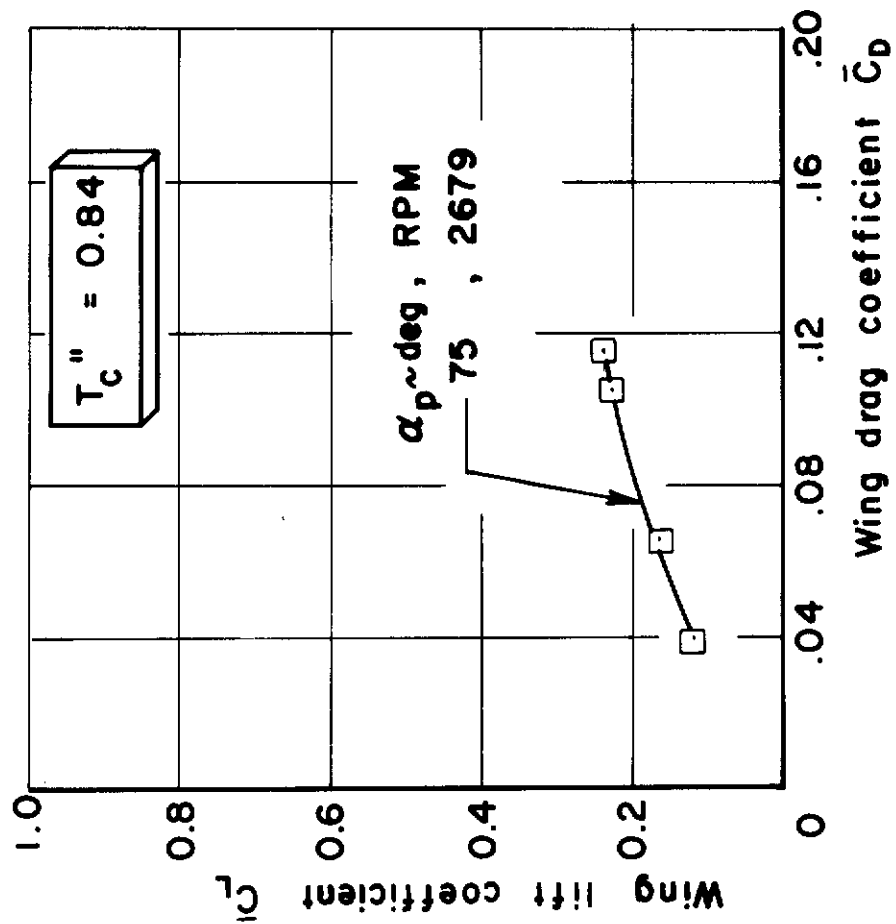


Fig. 12 continued. Drag polar.

Contrails

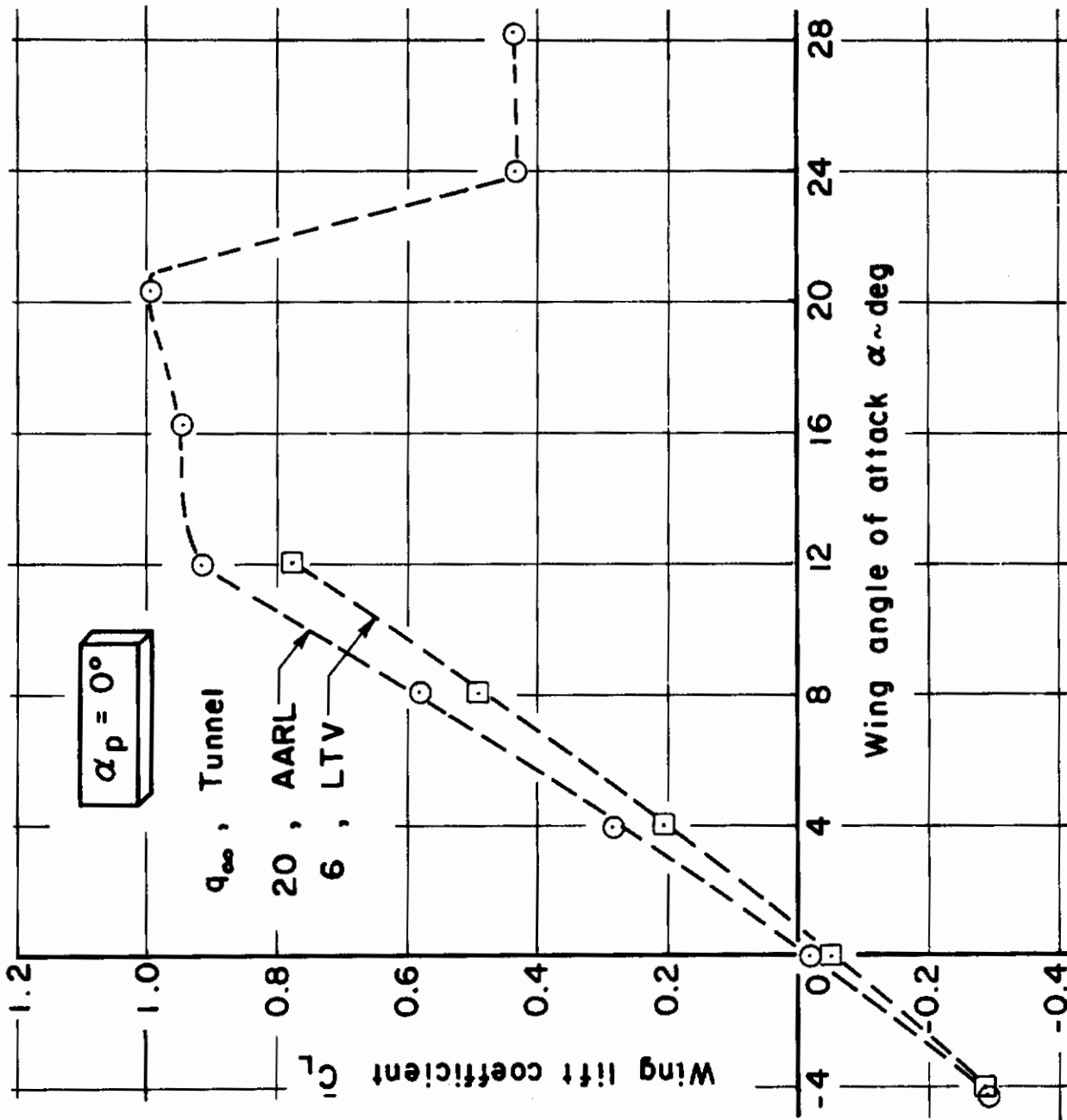


Fig. 13. Lift comparison at two different dynamic pressures in two wind tunnels (wing pinned, flap and slat retracted, propeller off, T.E. 1, $\delta_{123} = 0$).

T_c'' , q_∞

Wing free, 0.24-0.33, 2
 Wing pinned, 0, 20

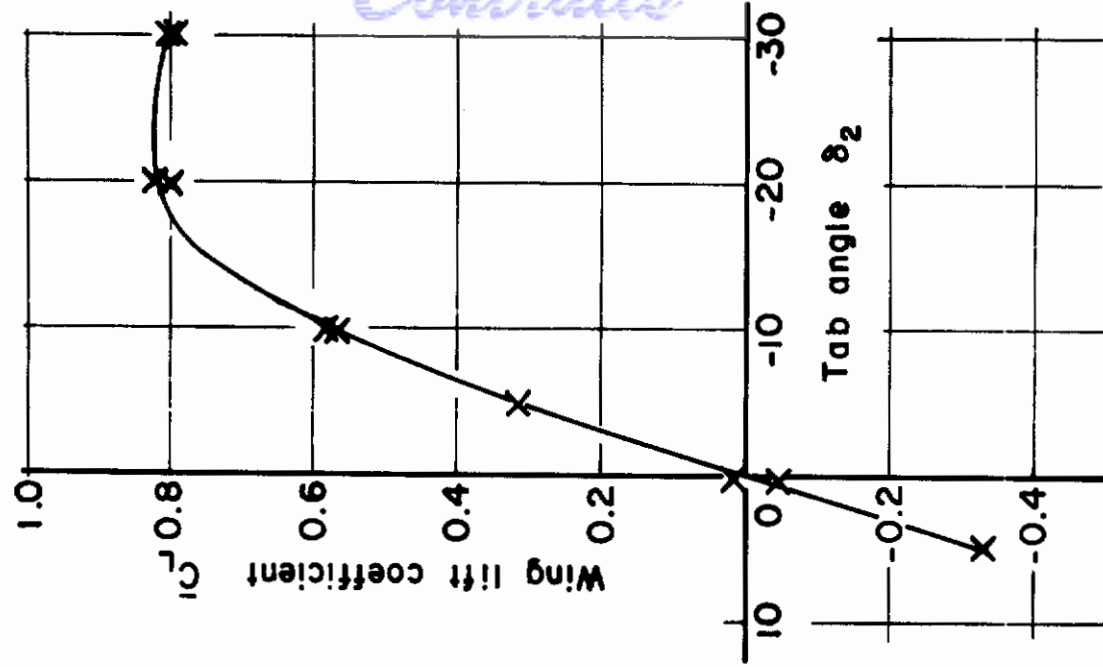
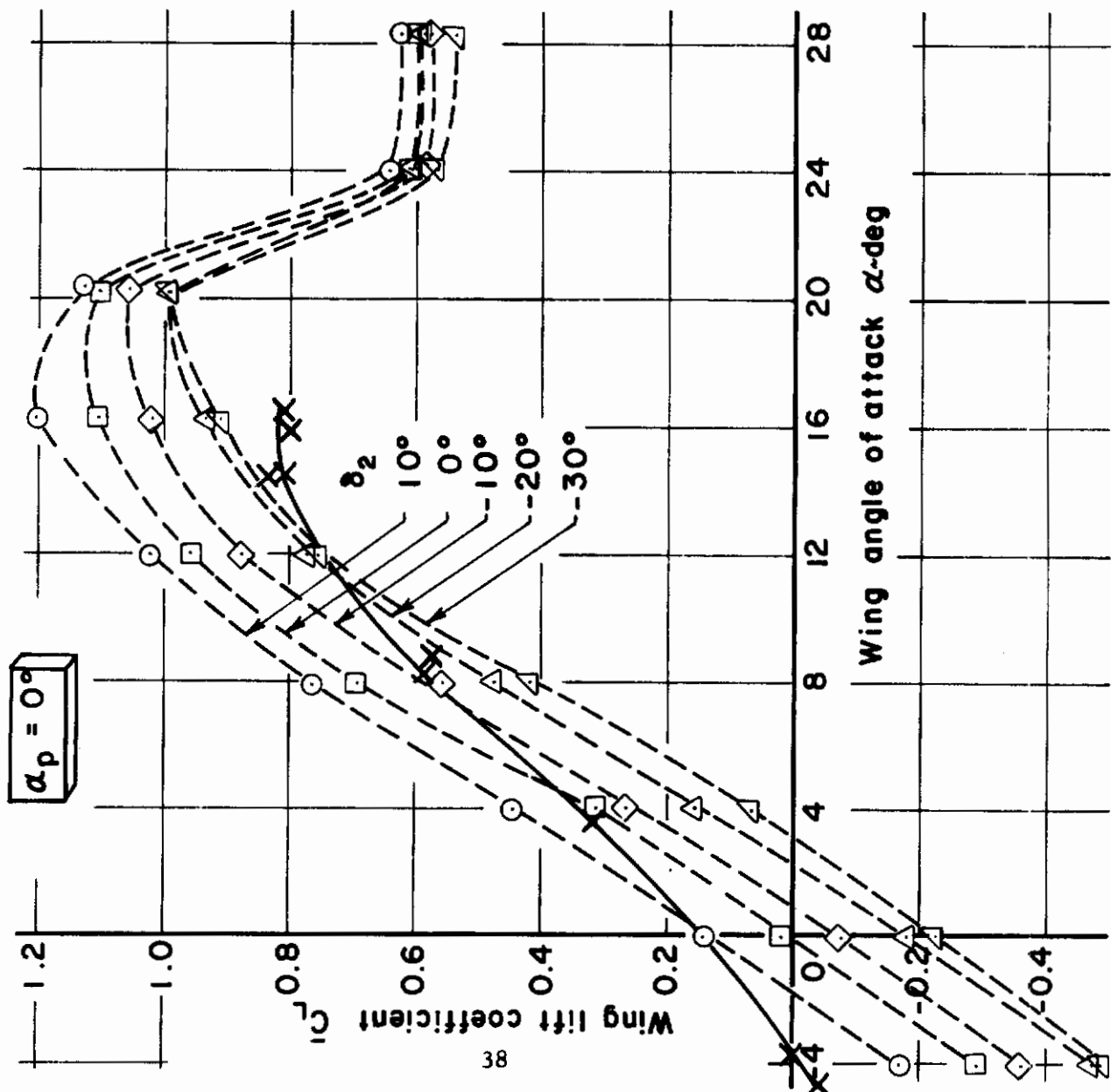


Fig. 14. Lift (flap and slat retracted, T.F. 3, $\delta_{13} = 0$, $Re_{pinned} \approx 0.82 \cdot 10^6$, pivot at 0.216c, AARL tunnel)

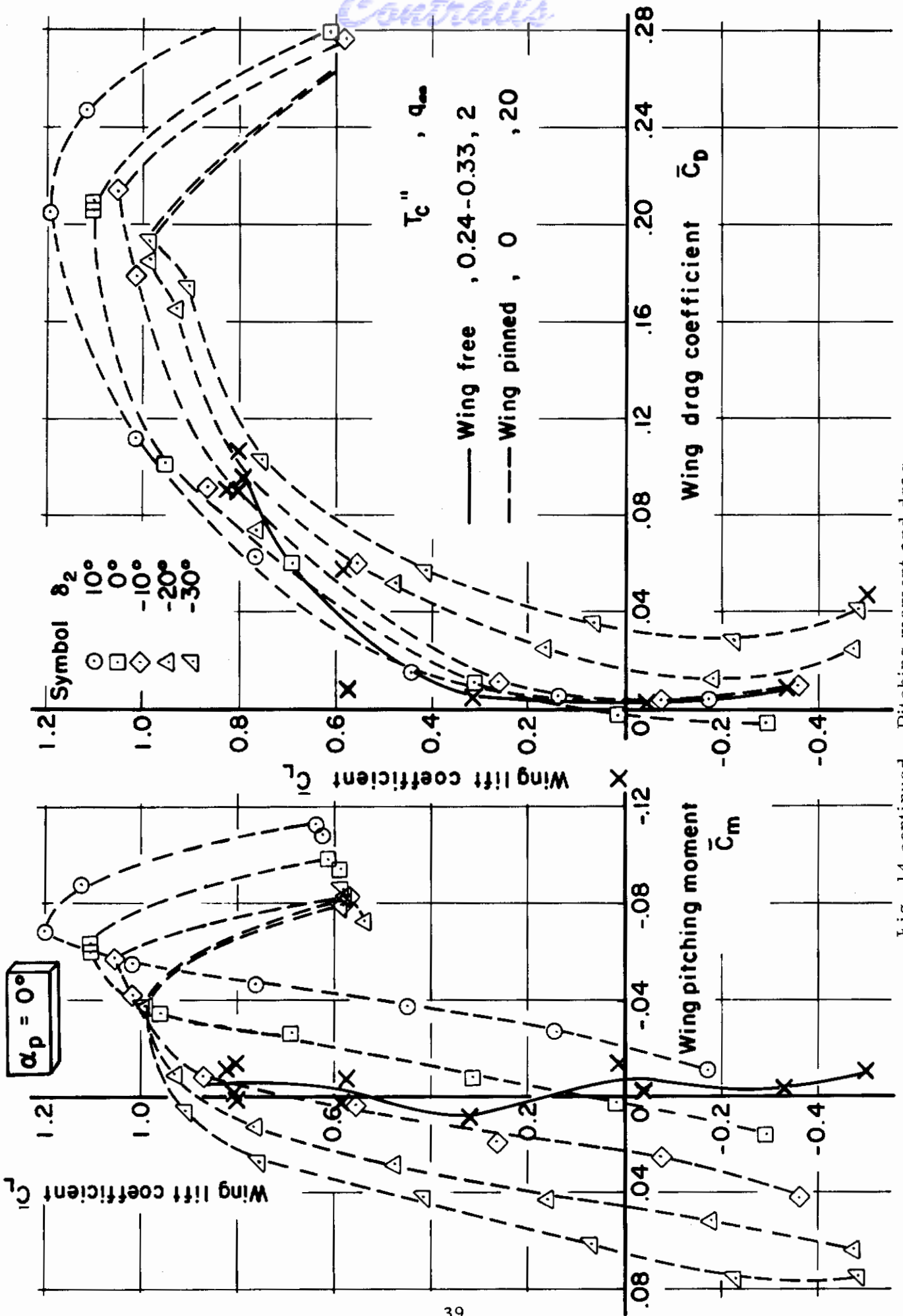


Fig. 14 continued. Pitching moment and drag.

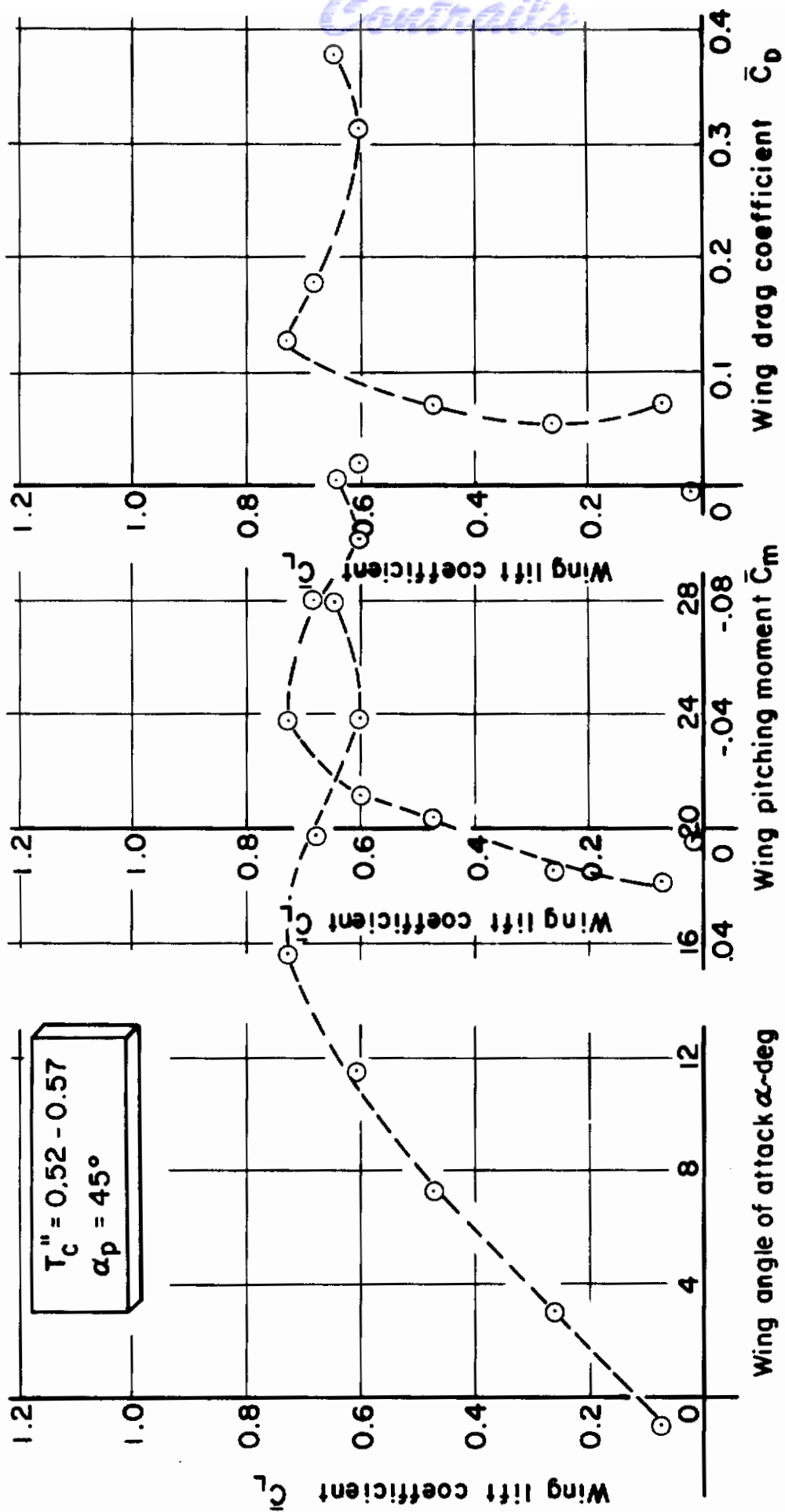


Fig. 15. Lift, pitching moment, and drag (wing pinned, flap and slat retracted, T. F. 3. $\delta_3 = 0^\circ$, $Re \approx 0.25 \cdot 10^6$, pivot at 0.216c, AARL tunnel, $q_{\infty} = 2$).

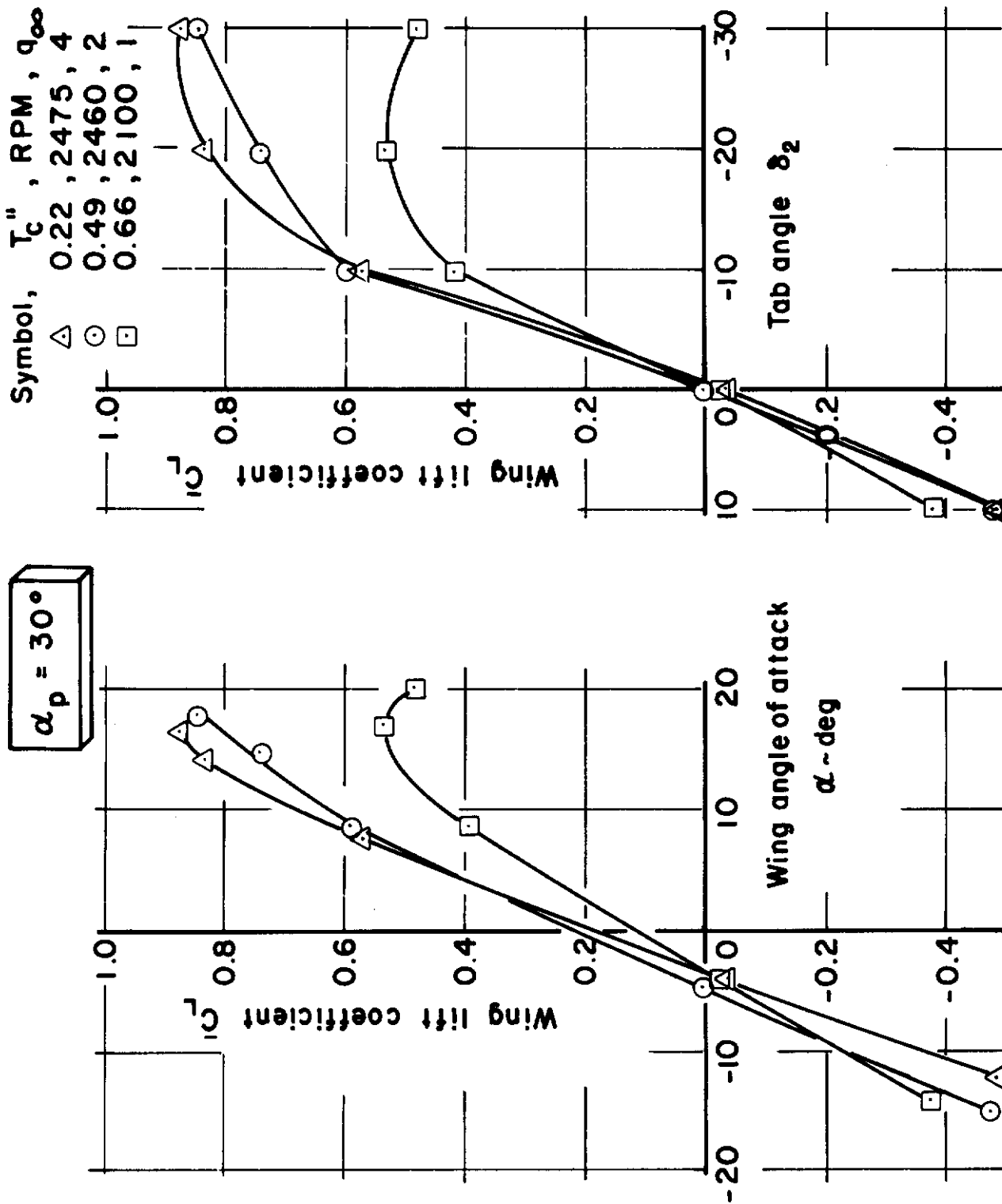


Fig. 16 Lift (wing free, flap and slat retracted, T.E. 3, $\delta_{13} = 0$, $Re \approx 0.3 \cdot 10^6$, pivot at 0.216c, AARL tunnel).

Symbol, T_c , RPM, q_∞
 \triangle 0.45, 2415, 3.5
 \square 0.60, 2355, 2
 \circ 0.75, 2280, 1

$\alpha_p = 60^\circ$

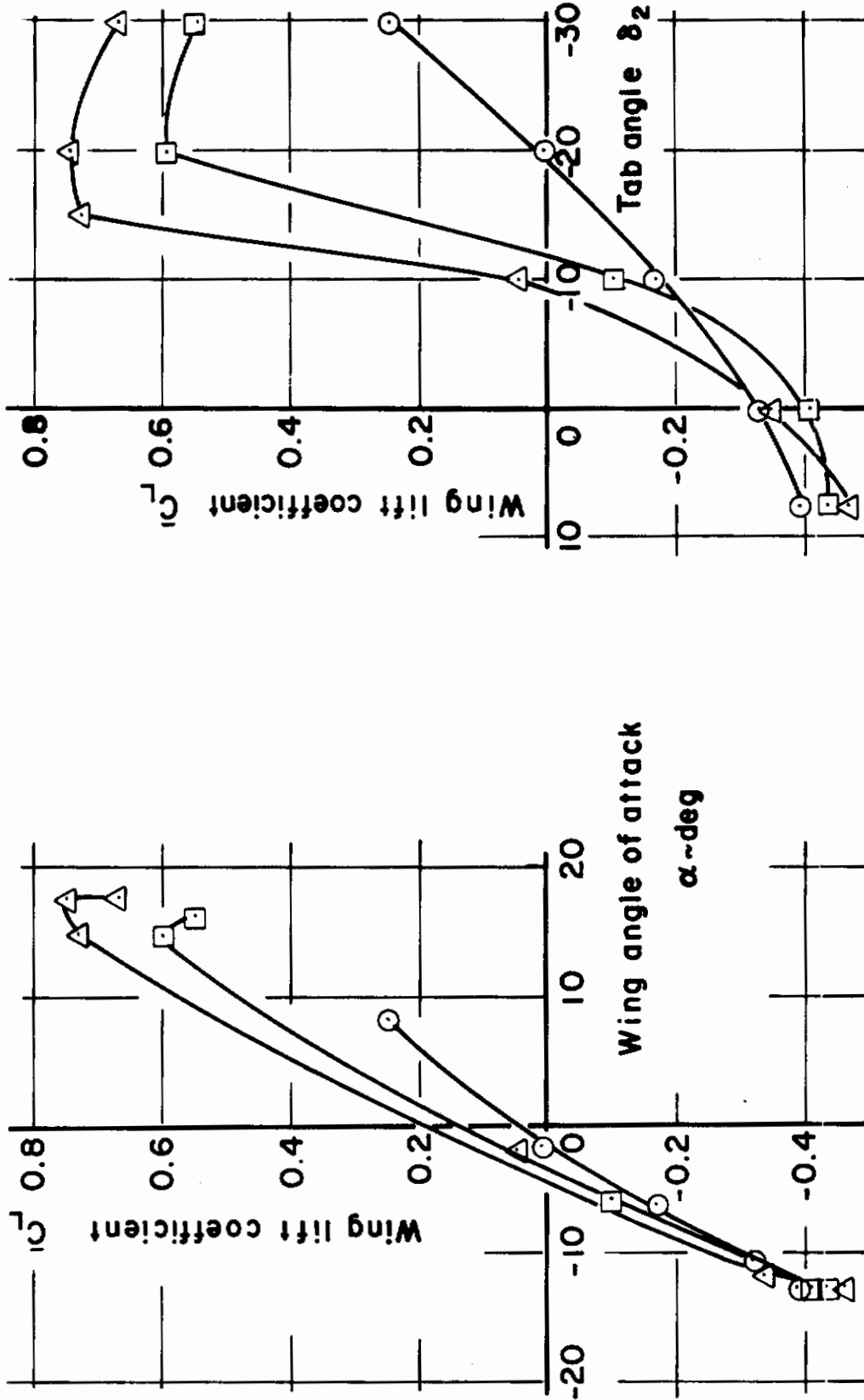


Fig. 17. Lift (wing free, flap and slat retracted, T.E.3, $\delta_{13} = 0$, $Re \approx 0.3 \cdot 10^6$, pivot at 0.216c, AARL tunnel).

Contrails

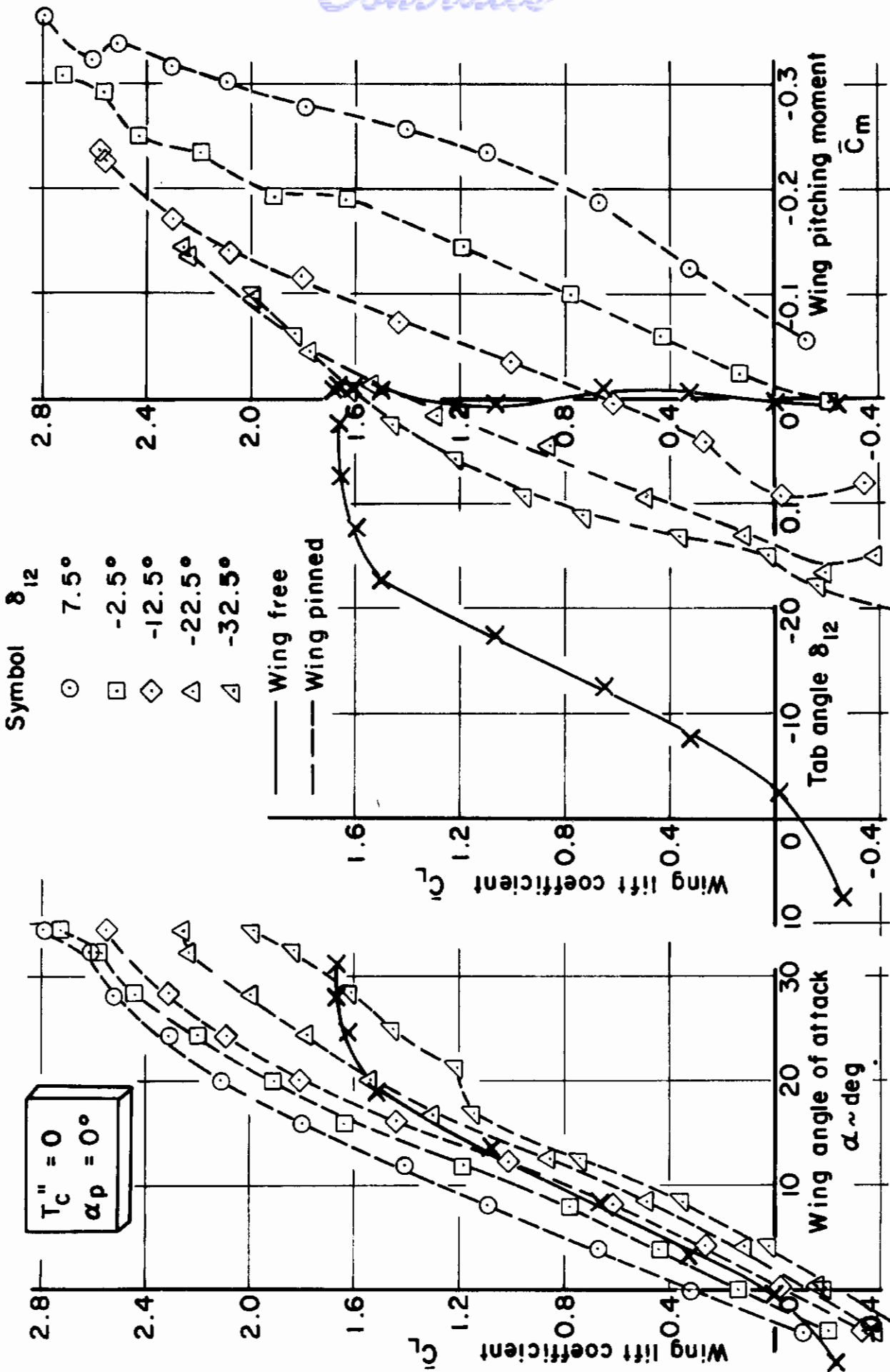


Fig. 18. Lift and pitching moment (flap and slat extended, propeller off, T. E. 4, $\delta_3 = -12.5^\circ$, $Re \approx 1.18 \cdot 10^6$, pivot at $\sim 0.22c$ extended, AARL tunnel, $q_\infty = 20$).

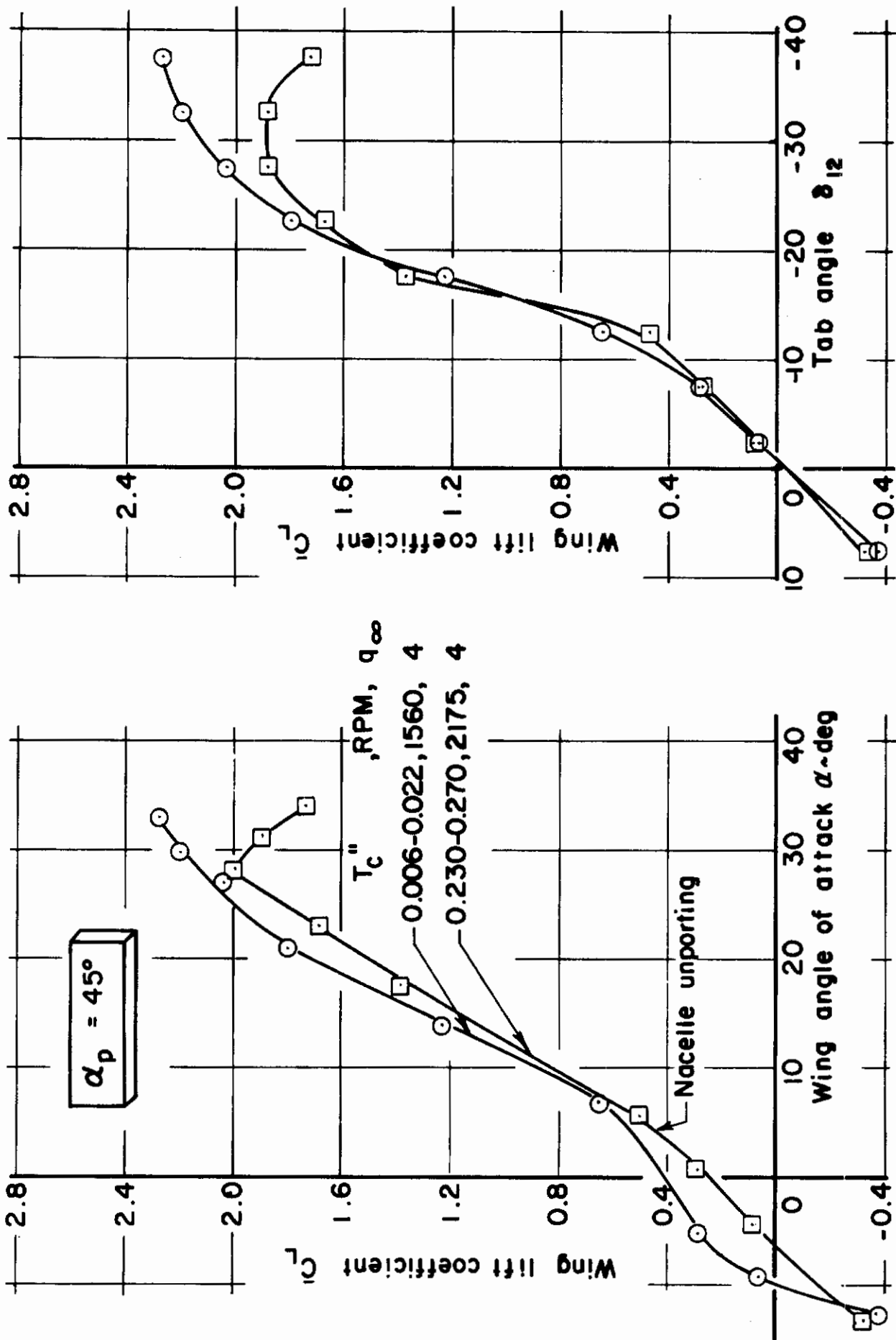


Fig. 19. Lift (wing free, flap and slat extended, T. E. 4, $\delta_3 = -12.5^\circ$, $Re \approx 0.52 \cdot 10^6$, pivot at $\approx 0.22c$ extended', AARL tunnel, $q_\infty \approx 4$).

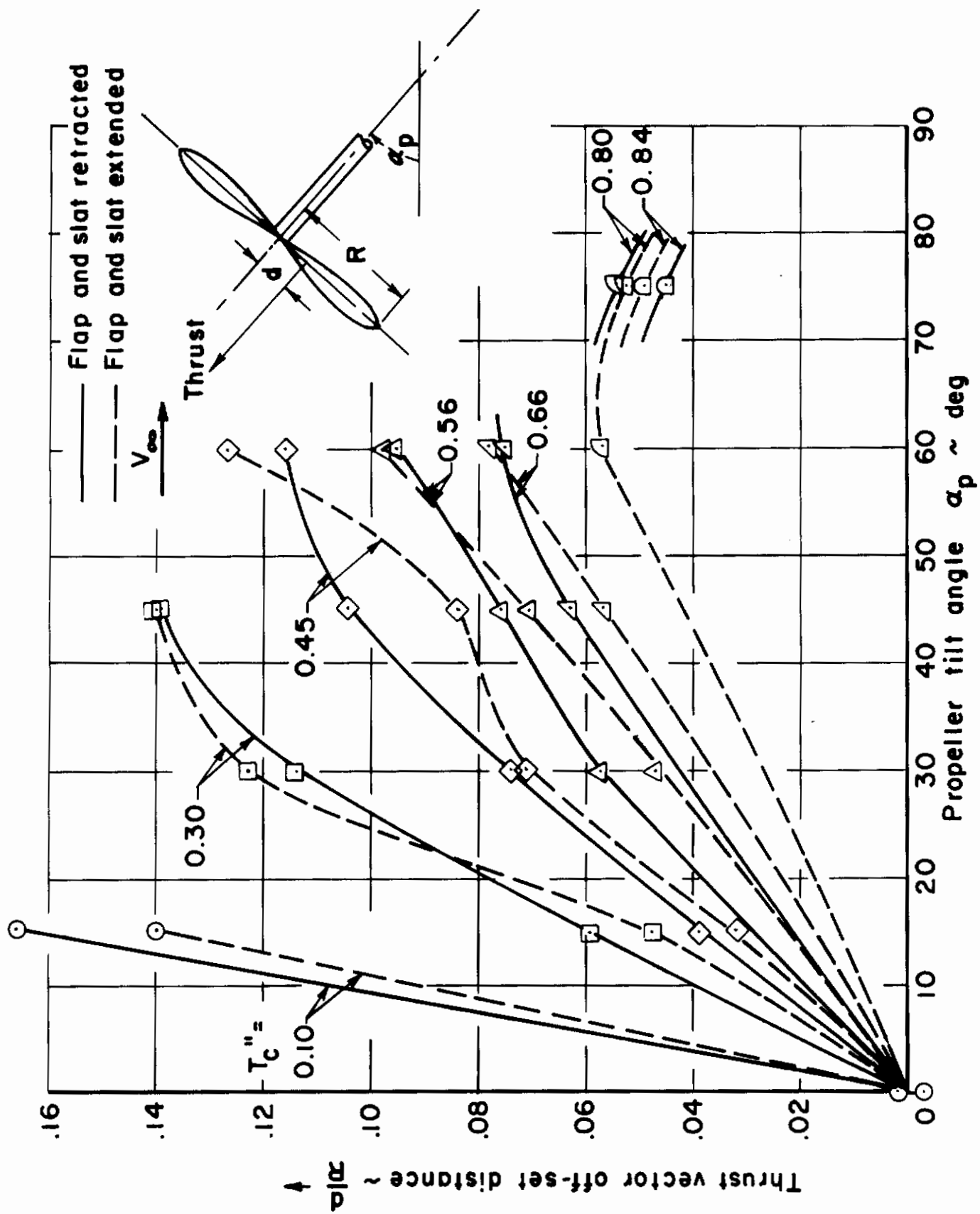


Fig. 20. Propeller thrust offset distance at angles of tilt.

Contrails

Contract AF 33615-C-1672 Distribution Lists

<u>Addressee</u>	<u>Copies</u>
Air Force Systems Command Wright-Patterson AFB, Ohio 45433	
ATTN: FDO-3 (STINFO)	1
" FDO-1 (Library)	1
" FDMM	10
" ASNPD-30	1
" SEPDE	1
" ASB	1
" APT	1
" ARD-1	1
" AFIT (Library)	1
DDC-TIAAS Cameron Station Alexandria, Virginia 22314	20
Secretary of the Air Force (SAFRD) Washington, D. C. 20330	1
Hq USAF (AFRSTF) Washington, D. C. 20330	1
AFCSAI Study Information Group Asst. Chief of Staff Studies and Analysis Hq USAF Washington, D. C. 20330	1

Contrails

AEDC ATTN: Technical Library Arnold AFS, Tenn. 37389	1
AF Missile Development Center Holloman AFB, N. Mexico 88330	1
Air University Library Maxwell AFB, Alabama 36112	1
DFSLB USAF Academy, Colo. 80840	1
AF Office of Scientific Research Washington, D. C. 20325	1
Air Force Systems Command Reference 1366 CA ATTN: SCS-41 Andrews AFB Wash, D. C. 20331	12
AFSC ATTN: SCTSM Andrews AFB Wash, D. C. 20331	1
Office of Aerospace Research ATTN: Technical Library United States Air Force Wash, D. C. 20333	1
DOL ATTN: Technical Library Bolling AFB Wash, D. C. 20332	1
AFSC STLO Langley Research Center (NASA) Langley AFB, Va. 23365	3
AFSC STLO Ames Research Center (NASA) Moffett Field, Cal. 94035	3

Headquarters US Army Material Command
Washington, D. C. 20315
ATTN: AMCRD-RP-A 1
AMCRD-DF 1

Chief of Research and Development 1
Dept. of the Army
ATTN: Physical Science Division
3045 Columbia Pike
Arlington, Va.

Chief of Research and Development 1
Department of the Army
ATTN: Air Mobility Division
Mr. John Beebe
Wash, D. C. 20310

Commanding Officer 2
US Army Aviation Material Laboratories
ATTN: SAVFE-PP
Fort Eustis, Virginia 23604

Commanding Officer 2
US Army Aviation Material Laboratories
SAVFE-AM
ATTN: W. E. Sickles
Fort Eustis, Virginia 23604

Headquarters US Army Research Office - Durham 1
ATTN: Technical Library
Box CM Duke Station
Durham, N. C. 27706

Commanding General 3
US Army Aviation Material Command
Admin. Services Office
ATTN: AMSAV-ADR
P. O. Box 209, Main Office
St. Louis, Mo. 63166

US Army Aeronautical Research Laboratory 2
ATTN: P. F. Yaggy
Moffett Field, Cal. 94035

Contrails

Chief of Naval Material (03L4) 1
Navy Department
Washington, D. C. 20360

Chief of Naval Material (0331) 1
Navy Department
Washington, D. C. 20360
ATTN: Mr. H. P. Santiago

Commander 1
Naval Air Systems Command (320)
Washington, D. C. 20360
ATTN: Mr. G. L. Desmond

Commander 1
Naval Air Systems Command (3032)
Washington, D. C. 20360
ATTN: Mr. F. W. S. Locke

Commander 1
Naval Air Systems Command (5301)
Washington, D. C. 20360
ATTN: Mr. William Kovin

Commandant 1
U. S. Marine Corps (AX)
Hq. U. S. M. C.
Washington, D. C. 20025

Commandant 1
U. S. Marine Corps (AX-5)
Hq. USMC
Washington, D. C. 20025
ATTN: Col. J. F. Paul

U. S. Marine Corps 1
Marine Corps Schools (CMCLFDA)
Quantico, Va. 22134

Chief of Naval Research 1
Navy Department
Air Programs Branch
Washington, D. C. 20325
ATTN: Mr. Dean Lauver

Commanding Officer and Director 1
Naval Ship Research and Development Center
Aerodynamics Laboratory (046)
Washington, D. C. 20007

Commanding Officer and Director 2
Naval Ship Research and Development Center
Aerodynamics Laboratory (635)
ATTN: R. Murphy, Washington, D. C. 20007

Contracts

Director Aeronautical Research NASA Wash, D. C. 20325	1
NASA Ames Aeronautical Laboratory Moffett Field, Cal. 94035	1
NASA Langley Aeronautical Laboratory Langley Field, Virginia 23365	1
NASA Lewis Flight Propulsion Laboratory Cleveland, Ohio 44118	1
Bell Aerospace Corporation ATTN: Technical Library P. O. Box 1 Buffalo, New York 14200	1
Boeing Airplane Company 7755 E. Marginal Way Seattle, Wash. 98108 ATTN: Technical Library	1
Cornell Aeronautical Laboratory, Inc. 4455 Genessee Street Buffalo, New York 14221 ATTN: Library	1
Douglas Aircraft Company ATTN: Max Klotzsche C1-23 3855 N. Lakewood Blvd. Long Beach, Cal. 90808	1
Douglas Aircraft Company 3000 Ocean Park Blvd. Santa Monica, Cal. 90405 ATTN: Technical Library	1
Grumman Aircraft Engr. Corporation ATTN: Library South Oyster Bay Road Bethpage, L. I., New York 11714	1

Contracts

Lockheed Aircraft Corporation California Division 2555 N. Hollywood Way Burbank, California 91502	1
McDonnell Aircraft Corporation ATTN: Library P. O. Box 516 St. Louis, Missouri 63100	1
North American Aviation, Inc. ATTN: Library International Airport Los Angeles, Cal. 9000	1
Northrop Corporation Norair Division ATTN: Library 1001 E. Broadway Hawthorne, Cal. 90250	1
Republic Aviation Corporation ATTN: Library Farmingdale, L. I., New York 11735	1
United Aircraft Corporation Research Laboratories ATTN: Library 400 Main Street East Hartford, Connecticut 06118	1
Bell Helicopter ATTN: Library P. O. Box 482 Ft. Worth, Texas 76101	1
Sikorsky Aircraft ATTN: Library Stratford, Conn. 06497	1
Boeing-Vertol ATTN: J. Liva P. O. Box 16858 Philadelphia, Penn. 19142	1

DOCUMENT CONTROL DATA - R & D

(Security classification of title, body of abstract and indexing annotation must be entered when the overall report is classified)

1. ORIGINATING ACTIVITY (Corporate author) Air Vehicle Corporation	2a. REPORT SECURITY CLASSIFICATION Unclassified
	2b. GROUP

3. REPORT TITLE

Wind Tunnel Tests of a Free-Wing Tilt-Propeller V/STOL Airplane Model

4. DESCRIPTIVE NOTES (Type of report and inclusive dates)
Aeronautical Research Report

5. AUTHOR(S) (First name, middle initial, last name)

T. Strand and E. S. Levinsky

6. REPORT DATE October 1969	7a. TOTAL NO. OF PAGES 47	7b. NO. OF REFS 6
------------------------------------	----------------------------------	--------------------------

8a. CONTRACT OR GRANT NO. F33615-68-C-1672 b. PROJECT NO. c. d.	9a. ORIGINATOR'S REPORT NUMBER(S) Report No. 360
	9b. OTHER REPORT NO(S) (Any other numbers that may be assigned this report) AFFDL-TR-69-80

10. DISTRIBUTION STATEMENT

This document has been approved for public release and sale; its distribution is unlimited.

11. SUPPLEMENTARY NOTES	12. SPONSORING MILITARY ACTIVITY Air Force Flight Dynamics Laboratory and Aerodynamics Laboratory, U.S. Naval Ship Research and Development Center
-------------------------	--

13. ABSTRACT

Wind tunnel tests have been conducted on a free-wing tilt-propeller V/STOL airplane model to investigate the aerodynamic characteristics of the free-floating wing in the propeller slipstream through the transitional region from cruise to near hover. Lift and drag curves wing-free have been obtained as a function of propeller tilt angle and thrust coefficient, and are compared with wing-pinned data.

The results indicate that the tilted propeller does not significantly turn the flow past the wing, except at thrust coefficients near unity and at propeller tilt angles near 90°. It is found that lift curve slope and maximum lift coefficient are strong functions of thrust coefficient. Provided the cruise static margin is adequate, the free-floating wing with flap and slat retracted behaves in the slipstream with no unusual problems. Based upon these initial test results, the free-wing concept therefore appears to be feasible aerodynamically. Additional wind tunnel tests are required on the free wing with flap and slat extended.

This document has been approved for public release and sale; its distribution is unlimited.

Unclassified

Security Classification

14 KEY WORDS	LINK A		LINK B		LINK C	
	ROLE	WT	ROLE	WT	ROLE	WT
V/STOL airplanes						
Tilt prop/rotor airplanes						
Fluid mechanics						
Wind tunnel tests						
Free-wing airplanes						

unclassified

Security Classification